Rational design and characterization of nitric oxide biosensors in E. coli Nissle 1917 and Mini SimCells

Rational design and characterisation of nitric oxide biosensors in *E. coli* Nissle 1917 and mini SimCells

Xiaoyu. J. Chen[a], Baojun Wang[b,c,d], Ian P. Thompson[a], Wei E. Huang[a*]

[a]Department of Engineering Science, University of Oxford, Parks Road, Oxford, OX1 3PJ, United Kingdom

[b]Hangzhou Innovation Center and College of Chemical & Biological Engineering, Zhejiang University, Hangzhou 311200, China

[c]School of Biological Sciences, University of Edinburgh. G20 Roger Land Building, The King's Buildings, Edinburgh EH9 3FF, United Kingdom

[d]ZJU-UoE Joint Research Centre for Engineering Biology, Zhejiang University, Haining 314400, China

*Corresponding author:

Wei E. Huang

Department of Engineering Science, University of Oxford, Parks Road, OX1 3PJ, Oxford, United Kingdom.

Tel.: +44 1865 283786

Email: wei.huang@eng.ox.ac.uk

Running title: Nitric oxide biosensors in mini SimCells and *E. coli* Nissle 1917.

Keywords: synthetic biology, mini SimCell, minicells, nitric oxide biosensors, NorR regulatory circuits.

Abstract

Nitric oxide (NO) is an important disease biomarker found in many chronic inflammatory diseases and cancers. A well characterised nitric sensing system is useful to aid the rapid development of bacteria therapy and synthetic biology. In this work, we engineered a set of NO responsive biosensors based on the PnorV promoter and its NorR regulator in *norRVW* operon, the circuits were characterised and optimised in probiotic *E. coli* Nissle 1917 and mini SimCells (minicells containing designed gene circuits for specific tasks). Interestingly, the expression level of NorR displayed an inverse correlation to P_{norV} promoter activation, as a strong expression of NorR regulator resulted in a low amplitude of NO inducible gene expression. This could be explained by a competitive binding mechanism where the activated and inactivated NorR competitively binds to the same site on the P_{norV} promoter. To overcome such issue, the NO induction performance was further improved by making a positive feedback loop that fine-tuned the level of NorR. In addition, by examining two integration host factor (IHF) binding sites of the P_{norV} promoter, we demonstrated that the deletion of the 2nd IHF site increased the maximum signal output by 25% (500 μM DETA/NO) with no notable increase in the basal expression level. The optimised NO sensing gene-circuit in anucleate mini SimCells exhibited increased robustness against external fluctuation in medium composition. The NO detection limit of the optimised gene-circuit pPnorVβ was also improved from 25.6 nM to 1.3 nM in mini SimCells. Moreover, lyophilised mini SimCell can maintain function for over two months. Hence, SimCell-based NO biosensors could be used as a safe sensor chassis for synthetic biology.

Introduction

One important goal of synthetic biology is to rationally design genetic circuits to reprogram living bacterial cells to perform specific human desired tasks[1]. Many advancements have been made in designing probiotics chassis for medically relevant purposes, such as programming *E. coli* bacteria to actively seek and kill detect pathogen[2], localise tumour and trigger self-lysis to release therapeutic cargo upon reaching critical density[3], decorate antigens for inducing cancer-specific immune response[4]. The functions of all these complex functions rely on robust and highly sensitive input modules, which can be coupled with external control methods (Gamma-ray[5], aspirin[6] or ultrasound[7]) for adjusting gene expression with precise spatial and temporal control. Alternatively, input modules can be used as sensing switches towards disease-related biomarkers or microenvironments[8], thus apply treatment or diagnosis at *in situ* levels[9,10]

Nitric oxide (NO) is a water-soluble (solubility 1.9 mM at 20 ^{o}C)[11], free radical gaseous small molecule that plays an essential role in human physiological functions and diseases[12]. An increased level of nitric oxide is often detected in many chronic inflammatory bowel diseases[13] and tumour progression[14]. NO exhibits a protective effect in the early development of various arterial diseases[15]. It also plays an essential role in host signalling between the gut microbiome and immune system[16]. Because of its prevalence and essential biological importance, a nitric oxide sensor would have enormous potential for *in-situ* diagnosis and condition-triggered drug release. It could also assist to further decipher the precise dynamics within host-microbiome interaction and enable *in vivo* tracking of disease progression, among existing transcriptional nitric oxide sensing pathways such as *soxR*, *oxyR*, *fur* and FNR[17,18]. P_{norV} and its NorR regulator in *norRVW* operon system have been reported to show a high sensitivity (~nM), specificity and degree of change in response to nitric oxide[19, 20]. Memory circuits have been developed based on the NorR regulatory system to record gut inflammation in the mouse model[21]. These circuits

demonstrate a sensing range of 30~100 μM in response to a nitric oxide donor DETA/NO (diethylenetriamine/nitric oxide) and validated functional in inflamed mouse ileum explants[21]. Although a plethora of studies characterised the activation mechanism and the effects of NorR binding site modification[22,23], few investigations focus on rational gene-circuit designs, the effect of NorR expression level and integration host factor (IHF) binding site of P_{norV} promoter. In this study, we characterised how the expression level of NorR can affect the sensory response, followed by fine-tuning of the dynamic range through promoter and feedback loop design. Based on the experimental data, we proposed a competitive binding mechanism to explain the NorR transcriptional regulation and used a mathematical model to simulate the NO sensing performance. The redesigned NorR gene circuit was able to detect NO in a medical relevant range of 26 nM ~ 13.5 μM. We also demonstrated that the redesigned NorR system could circumvent the interference of the native gene network in the host and displayed high sensitivity and robustness in chromosome-free mini SimCells, which are anucleate minicells containing designed gene circuits.

Results

Competitive binding mechanism of NorR regulated gene circuits

P_{norV} promoter is a σ^{54} dependent promoter, regulated by NorR and induced by nitric oxide. Unlike the classic transcription activation in σ^{70}-dependent promoter, σ^{54}-dependent promoters often form a stable complex upon binding and is transcriptional inert[19]. In the case of NO-induced sensing system, it requires activated regulator NorR and ATP hydrolysis to trigger subsequent conformation change for initiating the transcription process. In Fig 1A, NorR forms a homo-hexamer ring with N terminus that binds the upstream bacterial enhancer-binding site (bEBs), C terminus interacts with the σ^{54} holoenzyme. Notably, DNA bending (~160°) was achieved by the binding of two integration host factors (IHFs) that enabling close contact

between the NorR hexamer and σ^{54} factors[24]. In its off state, the central AAA+ domain which confers the ATPase activity of NorR is silenced (Fig 1B). Upon nitric oxide binding with the non-haem iron centre of the GAF domain, AAA+ domain is exposed, allowing further ATP hydrolysis and transcriptional activation (Fig. S1B)[25 26]. The NorR regulator (100% similarity) and its corresponding promoter P_{norV} in *norRVW* operon (98% similarity) in *E. coli* Nissle 1917 (EcN) is very similar to conventional lab strains *E. coli* K12 (Table S2). The gene-circuits were initially designed using a simple regulatory and open-loop format (Fig. 2A), in which P_{norV} promoter was fused with a super-folder *gfp* (sfGFP), and *norR* cloned from EcN was under the control of constitutive promoters with different strengths (P_{roA}, P_{roC} and P_{roD})[27] (Fig. 2A). Due to the gaseous nature of nitric oxide, a well characterised nitric oxide-releasing donor Diethlenetriamine/nitric oxide (DETA/NO) was used as an inducer[28]. The gene circuits were activated by NO released from DETA/NO in the range of 1.5 ~ 200 μM and the minimum detection limit was 1.5 μM of DETA/NO (Fig. 2B).

The stronger promoter strength of the NorR expression, the weaker amplitude of the induced sfGFP (super folder GFP) expression in the steady state (Fig. 2B and 2C). The strongest promoter (P_{roD}) produced the lowest induction amplitude, in comparison with the medium strength (P_{roC}) and weak (P_{roA}) promoter (Fig. 2B and 2C). There was no apparent difference between OD growths in all three cases, as shown in Fig S1. This ruled out the possibility that the decrease in sfGFP output was caused by any additional burden of NorR overexpression. These results were consistent with the previous report on SalR regulated aspirin response[6], where the overexpression of the regulator SalR suppressed the overall amplitude of aspirin-induced expression. The overexpressed NorR, under a strong constitutive P_{roD} promoter, produced a high level of inactivated NorR (NorRr), which competitively occupied the NorR binding site on P_{norV} promoter and reduced the possibility of the binding of NO activated NorR (NorRa) (Fig. 2B and 2C). Hence, the gene circuit with P_{roD} promoter had the lowest amplitude

(Fig. 2), compared to that of P_{roA} and P_{roC}, which are 33.3 and 3.59 times weaker than P_{roD}[27], respectively. In the weak NorR expression, there was no detectable increase in the baseline level. This could be due to the formation of transcription inert complex. The RNAp complex required both the activated NorR and ATP hydrolysis to trigger subsequent conformation change on σ^{54} for initiating transcription (Fig. 1). Thus, this extra step in ATP hydrolysis ensured a tightly regulated system. Many other σ^{54} dependent promoters intrinsically had a minimal baseline, for instance, the well-characterised toluene promoters $P_{u\text{-}xylR}$[29,30] or pathogenicity regulon P_{hrpl}[31].

Mathematic model of competitive binding mechanism

To further validate the proposed competitive binding mechanism, a conceptual model was constructed to simulate the competitive binding behaviour of the gene-circuits with different constitutive strengths. (Fig.S2.) As previously reported[32], the time kinetics was described by two sets of ODEs functions. [NorR] denotes the concentration of the regulator, and [GFP] denotes as the fluorescence protein output.

$$\frac{d[NorR]}{dt} = \alpha - \delta_1[NorR] \qquad \text{Equation (1)}$$

For a simple regulated system, the production rate of a constitutive promoter strength is α, and. α_1, α_2 and α_3 are relative strengths of P_{roD}, P_{roC} and P_{roA} [27]. δ_1 and δ_2 are separately [NorR] and [GFP] decay rates. Given that NorR and GFP are stable proteins, $\delta_1 = \delta_2$, and the decay rate is mostly due to dilution effect caused by cell division.

$$\frac{d[GFP]}{dt} = S([NO],[NorR])\alpha_{norV} - \delta_2[GFP] \qquad \text{Equation (2)}$$

α_{norV} is P_{norV} promoter production rate for sfGFP. The regulating term $S([\mathrm{NO}],[NorR])$ describes the interaction between NorR, inducer nitric oxide and the P_{norV} promoter, which can be expanded as:

$$S([NO],[NorR]) = \frac{Kr}{Kr + [NorR]}\left(\frac{[NorR]}{[NorR] + KA}\frac{[NO]^n}{[NO]^n + Ka}\right) \quad \text{Equation (3)}$$

Where K_r and K_a are the binding affinities between NorR and P_{norV}, NorR and NO, respectively. More details can be found in supplementary info.

The strength of each constitutive promoter has been previously characterised in *E. coli* [27] and the ratio between each promoter was used for the simulations. The initial delay caused via DETA/NO hydrolysis and NO accumulation was accounted for 30 min. The conceptual model output verified the competitive binding mechanism (Fig S2), confirming that the overexpression of regulatory proteins would lower the overall amplitude of gene expression in activated gene regulation.

Architecture change of the gene circuits significantly improve the performance

To find the optimal tuning spot, an autoregulatory system was constructed with a positive feedback loop that tunes the level of NorR expression corresponsive to NO concentration. (Fig 3A). To obtain a higher fold of change and amplitude, we coupled the P_{norV} promoter with *norR* and *sfgfp* orf to form a positive feedback circuit. As shown in Fig 3, the gene circuit of the positive feedback with the same P_{norV} promoter displayed much greater induction (F.c~5) and higher amplitude (21,000 $\pm$ 677 RFU) (Fig. 3B), compared to the best case in open-loop format (P_{roA}) (F.c~4.5) and amplitude (8,344 $\pm$ 1,040 RFU) (Fig 2C and Fig S3). Unlike a simple regulation using a constitutive promoter for the constant NorR production, the level of activated NorR in positive feedback is tuned in response to the concentration of NO inducer. This provides a better performance in terms of induction amplitude.

After obtained the optimal construct layout, we further modified the binding site component in P_{norV}. According to the promoter annotation[22,17], P_{norV} promoter had two integration host factors (IHFs) (Fig. 3A, Fig S4). IHFs are a class of regulatory protein involved in maintaining DNA architecture and allows site-specific DNA bending[33]. The features of two IHFs were

investigated by removing one/both of the IHFs sites near the transcriptional start site. As shown in Fig 3B, the gene-circuit significantly reduced its sensitivity and was only induced in the millimolar (1 mM) range of nitric oxide when both IHFs sites (IHF1 and IHF2) were deleted ($P_{norVnull}$). However, when one IHF before σ^{54} binding site -12/-24 (IHF2) was deleted($P_{norV\beta}$), the fluorescence amplitude (19,591 ± 214 RFU) increased by ~29% in comparison with the native promoter (P_{norV}) (13,931 ± 193 RFU) under saturated concentration (500 μM DETA/NO). The baseline of $P_{norV\beta}$ promoter increased by ~ 10% (3,338 ± 67 RFU), compared to the native promoter P_{norV} (3,031 ± 50 RFU). This result confirmed that both IHFs participates in the NorR based transcriptional activation. However, IHF2 had minimal impact on the activation of the promoter P_{norV} and the leakiness level. These results are similar to previously report regarding the binding affinity between NorR and IHFs, that the IHF2 binding displayed a much lower affinity than the IHF1[34].

Several studies have revealed that alteration of spacer or base pair of any NorR binding leads to catastrophic failure for system induction [1935]. Thus, mutagenesis studies were not carried for the NorR binding site. A summary of the dynamic profile for each circuit was shown in Table 3. Overall, a simple architecture change using positive feedback loop and IHF removal of the promoter exhibited good sensitivity and dosage response at a low range of inducer DETA/NO from 1.5 μM to 61.2 μM, this final optimised closed loop construct has an 3-fold increased fluorescence amplitude (25,228 ± 1322 RFU) at steady state (500 μM DETA/NO) compared to the construct pProA (8,344 ± 840 RFU) (Fig 2C and Fig S3).

Host interference and circuit performance in Δ*norR* strains

Since NorR regulation involved a dynamic competitive binding mechanism, it was hypothesised that NorR from native chromosomal expression could also compete with NorR expression from the gene-circuits on the plasmid, leading to the lower output amplitude (Fig.

4A). We then investigated the impact of the native chromosomal *norR* on the performance of a gene circuit. Due to the low chromosome editing efficiency in EcN [36] and high similarity of *norRVW* operon it displayed with other communal *E. coli* strains (Table S2). *E. coli* DH5α was used as a proxy for this experiment, by comparing construct pPnorVβ in *E. coli* DH5α and its Δ*norR* mutant. As shown in Fig 4B, the results indicated that an increase of GFP amplitude by 69% in the Δ*norR* mutant when compared to *E. coli* DH5α under induction of 1 mM DETA/NO. The baseline leakiness also increased from 1,825 $\pm$ 8 RFU (wild type) to 3,128 $\pm$ 124 RFU (Δ*norR*) in 3h induction. The system exhibited a much higher fold of change (F.c ~12) in Δ*norR* mutant than the wild-type strains. (F.c ~5.4) (Fig. 4C). In both cases, the minimal sensitivity of DETA/NO was the same, 30 μM (Fig. 4B). This suggested that the host native expression of NorR could compete to bind $P_{norV\beta}$ promoter on plasmids and acts as a repressor to the expression of sfGFP (Fig. 4C). This further validated the proposed competitive binding mechanism of NorR regulation where NorR can not only be thought as the activator for P_{norV} but can also function as a strong repressor for tight regulation.

The performance of the optimised circuits in mini-SimCells

In order to bypass the interference of the native gene network in the host and create a non-dividing and safe NO biosensor, the performance of the gene circuit in purified mini SimCells was investigated. We cloned the optimised pPnorVβ construct into *E. coli* MC1000 $_{\Delta}$*minD* strain which can generate minicells due to the disruption of *minD* gene[37]. The abnormal division generated one cell with a duplicative chromosome and an anucleate minicell. Mini SimCells generated from Δ*minD* strain contained plasmids with designed gene circuits that have shown functional dose-response in the various system[6]. However, only σ^{70} dependent systems were tested in mini SimCells so far. Fig. 4 demonstrated that the chromosome-free minicells (mini SimCells) were able to express sfGFP by NO induction in a dose-response

manner. Through using an optimised protocol [37, 38], it was possible to retrieve highly purified SimCells culture with a yield of 5×10^9 mini SimCells/ml. Both OD600 measurement and plate assay confirmed that the purified SimCells were free of parent cell contamination. Plate assay was carried over 16 and 48 h to rule out any slow-growing parent cells (Fig. 5A). The relative fluorescence amplitude (sfGFP/OD) of the purified mini SimCells (19,077 ± 519 RFU) was approximately 8.6-fold less than that in the parent cell (164,100 ± 8161 RFU). This could be due to the small cellular volume of the mini-SimCell, which was about quarter of a typical *E. coli* cell[39] and much less than the filamentous *E. coli* Δ*minD* parent cells (5~40 μm). Furthermore, using an established formula for mini SimCell counting[38], fluorescence per cell per volume for mini SimCells ($3.5 \times 10^{-6} \pm 9.4 \times 10^{-8}$ /cell volume) was comparable to that of the parents cells ($3.1 \times 10^{-6} \pm 5.4 \times 10^{-8}$ /cell volume) (Fig. 5). Interestingly, the induction fold change in mini SimCells (F.c~24.5) was higher than that of parent cells (F.c~12.3), mini SimCells also displayed a lower detection limit of 1.5 μM of DETA/NO than the parent cells, 15 μM (Fig. 5A and S5). Furthermore, in contrast to a delay of 24 min observed in the parent cells under saturated inducer concentration (500 μM, Fig. 5A), mini SimCells showed much faster induction of 0.25 h (Fig. 5B). This indicated that mini SimCells can circumvent the interference of native gene network in parent cells but contained the machinery to express σ^{54} based transcriptional circuit with improved performance.

Mini SimCells bypassed physiology limitation of parent cells

From previous literature in the characterisation of σ^{54} dependent promoter family, it has been reported that σ^{54} related gene was commonly related to stress response, biofilm formation and flagellar movement[40]. In *E. coli*, almost half of the σ^{54} related gene associated with nitrogen assimilation[41] pathway were upregulated in nutrient starved conditions[42,43]. To investigate how the nitrogen depletion would impact the synthetic circuits, *E. coli* Nissle 1917 with pPnorVβ

gene circuit was tested in both PBS and M9 media. From Fig 6A and 6C, the circuits showed an apparent delay of 2 h when PBS medium was used for DETA/NO induction of parent cells. In contrast, DETA/NO induction of the parent cells in M9 medium demonstrated a much faster response to DETA/NO, similar to that in LB. (Fig. 2 and Fig. 3). Interestingly, the DETA/NO induction of mini SimCells showed an fast response (< 1h) under low level of induction (12.5 μM), independent of the medium type, as sfGFP expression exhibited similar induction kinetics in both PBS and M9 medium (Fig 6B).

Further testing in different carbon sources did not significantly alter the response time or the dynamic ranges (Fig. S6). Despite little difference was observed in OD growth (Fig. S7), this delay could have been due to the lack of a nitrogen source in PBS. Since P_{norV} is a σ^{54} dependent promoter and σ^{54} is related to nitrogen metabolism, it can be reasoned that under a relatively fixed number of RpoN factors in both log phase or stationary of the cells[44], upregulation of host nitrogen assimilation gene could have competed for the same transcriptional factor RpoN pool with the introduced gene circuits, thus leading to a time delay. RpoN (σ^{54}) only consists of 8% of the transcriptional holoenzyme (σ^{70} ~78%)[45], σ^{54}-dependent promoters might be more sensitive towards fluctuation of external nitrogen than other σ transcription dependent systems. Therefore, once the same gene circuit was introduced in mini SimCells, as shown in Fig 6B, nitrogen-free PBS had no impact on DETA/NO inducible sfGFP expression. The gene circuits could be triggered immediately in both PBS and M9 cases with a greater magnitude of induction ~10. This could have been due to the absence of competition of RpoN pool in anucleate mini SimCells.

Long-term storage of mini SimCells loaded with sensory gene-circuits

Lyophilization (freeze-drying) is a common approach for preserving biological compounds at room temperature for long-term storage and transportation[46]. To further explore the potential

application of mini SimCells, purified mini SimCells were lyophilised with the optimised nitric oxide sensing circuits (pPnorVβ) and kept at room temperature (~25 °C). After stored at room temperature for two months, the freeze-dried parent cells and mini SimCells were revived and examined. Fig 7 A and B demonstrated that both mini SimCells and parent cells maintained the detection sensitivity of 15 μM DETA/NO after revival. The freeze-dried parent cells exhibited a ~24-fold lower intensity (6,298 $\pm$ 100 RFU) (Fig. 7A) than the freshly transformed cells (151,700 $\pm$ .2615 RFU) (Fig. 5A). In contrast, mini SimCells exhibited a ~11-fold reduction in the output intensity (1,668 $\pm$ 32 RFU) compared to the freshly transformed mini SimCells (Fig. 7). This can be further calculated as $3.3 \times 10^{-7} \pm 6.3 \times 10^{-9}$ RFU/cell volume for the mini SimCells intensity and $2.1 \times 10^{-7} \pm 3.2 \times 10^{-9}$ RFU/cell volume. Nevertheless, NO induction could still be triggered within 2-h with a fold of F.c~10 for mini SimCells and F. c~15 for parent cells (Fig. 7C), respectively. Furthermore, mini SimCells still showed a slightly faster response time than the parent cells. The reduction in fluorescence output in mini SimCells might have been due to the loss of ATP regeneration machinery after long term storage.

Discussion

In this work, a series of nitric oxide biosensors have been constructed from *E. coli* Nissle 1917, Based on previous annotation of the E. coli *norVW* operon, in its native contexts, flavorubredoxin and its redox partner encoded by *norVW* are under the control of NorR and P_{norV}, the regulator NorR consists of a N-terminal regulator domain that responds to the NO signal through its non-haem iron centre[47]. In activation state, the NorR protein forms a homohexmer ring (n=6) over the P_{norV} promoter, such high cooperativity ensured its switch like behaviour upon NO triggering. Moreover, the NO scavenger (*norV*) as the product of *norR* activation removes the NO inducer over time and therefore, forming a negative feedback loop

which is a commonly found network motif that can speed up the response time[48]. Based on the knowledge, we focused on the P_{norV}/NorR interaction and redesigned it into a modular NO sensory circuit. We successfully demonstrated that the competitive binding mechanism could also apply to the σ^{54}-dependent NorR regulatory system, similar to σ^{70}-dependent SalR[6]. The binding of a regulatory protein and a promoter was a dynamic process, it was previously showed that the intracellular concentration of the regulator could drastically affect the system dynamics, in some cases amplified the transcriptional signal[49]. However, depending on the interaction between regulatory protein and the inducer, we found the regulatory protein NorR can either be in its activated (NorRa) or inactivated/repressive state (NoRr). The competitive binding mechanism proposed assumes that both activated and inactivated regulatory proteins are able to bind the same site of the promoter. This is supported by previous studies where an iron cluster truncated NorR mutant failed to respond to NO level yet still repressed the promoter activity[25]. The transport of NO into *E. coli* is mainly through diffusion [50]. However, *E. coli* has multiply highly efficient NO scavengers such as nitrogen dioxygenase (NOD) and flavorubredoxin (NorV) that protect the cells against oxidative damage [51]. Upon overexpression of the regulatory protein under limited intracellular inducers, the non-bound form of NorR actively competes and occupied the binding site of the promoter, so it represses the frequency of subsequent gene expression. No additional cellular burden incurred was noted (Fig S1). This provides a potential universal tuning strategy applicable to different transcriptional regulations for modulating the dynamic range by merely rearranging the design architecture or the strength of regulator expression.

The detection limits of parent cells and mini SimCells gene circuits was 15 μM and 1.5 μM of DETA/NO (up to ~ 500 μM) respectively (Fig 2 and 3). Based on established NO release dynamics model of DETA/NO [28] and *in vitro* quantified release[52], a linear correlation was calculated for the total nitric oxide released within the first three hours and the DETA/NO

concentration. Only the first three hours were used for calculating the integrated area under the curve since this is the time take to fully activate the system. We estimated that the actual released NO detection limit of gene-circuit pPnorVβ was 25.6 and 1.3 nM in parent cells and mini SimCells, respectively. The operational range of the optimised circuits (25.6 nM ~ 13.5 μM) fitted well with the medical relevant pathogenic threshold detected in active ulcerative colitis (UC) (>17.4 μM), inflammatory bowel disease IBD (>13.7 μM) and chronic inflammatory diseases (>14 μM)[13,53]. This was in good agreement with previous reports of NorR response to the nM scale of nitric oxide[54]. Furthermore, the initial lag in response (30 min~ 1 h), as we observed in circuits activation, could have been due to the time required for NO release from DETA. Thus, the true activation time for NorR regulatory system could have been much shorter.

To address how other promoter modules affected the overall response dynamics, two of its IHFs sites were investigated (Fig 3). By rationally redesigning the IHFs site, we demonstrated that the modified IHF2 site was not essential to the induction performance. Instead, the deletion enabled a 29% increase of the GFP amplitude with no significant baseline increase (Fig 3B). In contrast, the 1st IHF was found to be critical for system induction. It was evident that the 1st IHF is essential for bringing close contact of the NorR regulator and σ^{54} core enzyme [25]. Considering the 2nd IHF displayed a much lower affinity than the 1st IHFs site[17] and the previous evidence suggested its role in transcription inhibition[34]. The results confirmed the function of 2nd IHF *in vitro* and provided a minimal version of the P_{norV} promoter ($P_{norV\beta}$) with ideal induction characteristics (Fig 3B). It is worth mentioning that this unique IHF binding block might be useful for rationally designing tightly regulated σ^{54} chimeric promoters for the future.

From a practical standpoint, the results of this study confirmed that the optimised NorR constructs could be triggered by 15 μM of DETA/NO within 30 min. Such a rapid response

time and high sensitivity confirmed its potential in applications such as an *in-situ* disease triggered sensor when loaded in *E. coli* Nissle 1917. The traditional methods such as Griess assay or indirect assays measuring the NOS activity cannot be used in the *in vivo* setting or lack of accuracy[55]. Other electrochemical methods do offer higher sensitivity down to 1 nM and much faster response (~sec), but it cannot offer a monitoring of NO at the cellular level *in-situ* [56]. The transcriptional circuits described in this study are highly modular and can be adapted to different type of sensor outputs such as luminescence or fluorescent protein while offering nM detection limit at the same time.

Furthermore, because of the importance of NO as a signalling molecule in human-microbiome communication[16] and plant pathogen response[57], the NO biosensor could be used as a direct *in vivo* probe in studies of interspecies communication, which rely on S-nitrosylation[58]. For instance, it was previously shown the microbiome-derived NO promotes widespread S-nitrosylation of the host proteome[16] and subsequently altered protein function. However, the detailed kinetics and timing of NO release remained unknown. For *E. coli* Nissle 1917, a probiotic strain which can transiently colonise the human gut for two weeks[59], together with our sensory systems could provide enough time for measuring the NO dynamics when coupled with acoustic reporter for real-time *in vivo* tracking[60]. Nevertheless, a recombinase based cellular memory circuit or oscillatory circuit can also be added to quantify and record the incidence of NO exposure in faeces or biopsy samples[21,61]. The sensor developed here can cope a wider sensing range of 15 μM ~ 500 μM DETA/NO compared to the most recent published one that has a range of 30 μM ~100 μM[21]. To improve the diagnosis specificity, an AND logic gate sensing design can be built in combination with our modular sensor, such as using ThsS/ThsR based tetrathionate and thiosulfate sensor which are both in-direct biomarkers for gut inflammation[62]. For *in vitro* testing using human blood or urine samples, which have demonstrated growth inhibitory effect towards bacteria cell [10], the use of mini-SimCells NO

sensors would be an alternative, not only bypassing the growth coupling and related drawbacks, but also could exhibiting increased induction fold and lower detection limit (Fig. 5 and 6).

Host interference is one of the significant bottlenecks in whole-cell biosensor applications. The fluctuation in biosensor expression as a consequence of changes in medium conditions (carbon/nitrogen) has been previously reported for other σ^{54}-dependent systems[30,63]. From previous studies characterised the *Pu* promoter, which was also an σ^{54} dependent promoter[30], have highlighted that such systems suffered from intrinsic exponential silencing when placed in a rich medium (LB broth). However, this was not the case in a cell-free state when supplied with separate IHF, σ^{54} and core RNAPs[64]. The NorR system detailed here did not display such a delay in LB. However, the system exhibited a response delay when supplied in nitrogen depleted medium (PBS) (Fig 6A). This could be attributed to a competition for the limited σ^{54} pool, which corelates well with the fact that all the nitrogen assimilation gene are upregulated (*Ntr* regulon)[65] during nitrogen depletion. Due to the σ^{54} factor only contributed a small sharing pool (~8%) of the total transcriptional factors, this makes the NorR circuits activation strongly dependent of the cellular contexts when σ^{54} is limited. Such explanation is also supported in other studies where the promoter sequence spanning -12/-24 (σ^{54} binding site) were found to be the rate limiting step and involved in growth condition coupling.[66,67]. As part of the host interference, it was demonstrated that *norR* in the chromosome of *E. coli* acted as a strong repressor for the gene-circuits. The gene circuits were examined in *E. coli* DH5a due to low chromosome editing efficiency in EcN (data not shown). Despite both strains possess highly similar *norWV* operon, for future improvement, the newly modularised endogenous cryptic plasmids (pMUT1 and pMUT2) of EcN might offer a convenient platform for chromosome editing and metabolic rewiring when used in combination with dCas9 [68]. This new system could allow us to investigate the effect of host *norR* copy in a more accurate cellular context.

To decouple the host interference and the reliance of σ^{54} pool, one potential strategy is to supply an extra copy of σ^{54} on the cryptic plasmids, this might lead to unexpected global regulatory change in the host cells. An alternative solution, to overcome such limitations in cellular context-dependence and make the sensing system more robust is to use another type of SimCells which remove the host chromosome while maintain its core transcriptional and translational machinery[69]. The *E. coli* adapted minicells proposed here which is chromosome-free, nanosized cell chassis demonstrated increased sensitivity and response speed with loaded NO sensing circuits. Such a strategy is advantageous in handling complex organisms which developed many evolution redundancies that do not fit the application niche. Finally, we have tested for the first time the long-term storage of freeze derived mini SimCells loaded with synthetic biosensor constructs. The results demonstrated an acceptable shelf-life with room to improve, this could pave ways for future development of mini SimCell biosensor on paper diagnostics for analysing gut microbiota and host biomarkers[70]. These results collectively exemplified a mini SimCell loaded NO sensor with enhanced safety, robustness and sensor performance. In summary, we provided a simplified NorR based NO transcriptional circuit with optimised dynamics and validated its performance in both mini SimCells and probiotic EcN for aiding the rapid development of bacteria therapy and synthetic biology.

Materials and methods

Chemicals, medium and growth conditions

All chemicals were purchased from Sigma-Aldrich unless otherwise noted. Nitric oxide inducer is purchased under CAS number 146724-94-9 Diethylenetriamine/nitric oxide (DETA/NO). *Escherichia coli* DH5α was routinely used for molecular cloning and plasmid maintenance. Final optimised constructs were tested in probiotics strain *E. coli* Nissle 1917 (*E. coli* Nissle 1917), obtained from Ardeypharm GmbH (Herdecke, Germany). For normal cell

growth, bacteria were inoculated from a colony and grow in Luria-Bertani (LB) broth with corresponding antibiotics kanamycin (60 μg/mL); Ampicillin (100 μg/mL) and incubated at 37 °C, 250 rpm for 16 h. For the carbon/nitrogen experiments, the M9 medium was made from M9 5x minimal salts (Sigma-Aldrich) supplemented with carbon sources and corresponding antibiotics. PBS medium was made from 5 g of Gibco tablets dissolved in 500 mL of deionised water. SOC medium was made according to CSH protocol (cshprotocols.cshlp.org)

Gene circuits synthesis & cloning

All protocols were carried out with enzymes obtained from New England Biolabs (NEBs), and all primers were synthesised by Sigma-Aldrich. Standardised backbone vector pGEMT (Promega) and pMK (GeneArt) were used for all constructs with ColE1 ori (15~20 copy/cell). A strong ribosome binding site (AAAGAGGAGAAA) (BBa_B0030) was used for both *sfGFP orf* and *norR orf.* A strong bidirectional terminator (BBa_B0020) was attached after the stop codon for insulation. All plasmids in Table 1 were designed and then synthesised using the GeneArt cloning service. For deletion of IHF of the P_{norV} promoter, primers designed shows in Table S3 and standard Gibson cloning was carried out using NEB Hi-Fi assembly kit. The original *norR* sequence and P_{norV} sequence was retrieved from *E. coli* Nissle 1917 (GenBank No. CP007799.1). Sequence info and plasmids map are provided in supplementary info (Table S4, S5 and Fig S8).

To generate *norR* mutant strains, molecular cloning was carried out as follows. P1 phage transduction method was used to generate *E. coli* MC1061 Δ*norR* knockout strain in this study, and the *ΔnorR* strain from Keio collection was used as a donor for the gene knockout cassette. Kanamycin resistance marker was then excised from the host-strain chromosome using the method described previously[71]. Briefly, transduced strains were made electrocompetent and transformed with the plasmid, pCP20. Transformants were grown overnight at 30 °C in Luria

Bertani (LB) medium supplemented with 100 μg/mL ampicillin. The resulting cultures were plated on LB agar medium and grown at 42 °C. Individual colonies were tested for ampicillin and kanamycin sensitivity. The gene deletions and subsequent kanamycin marker removal were verified by the polymerase chain reaction

Bacterial transformation of E. coli Nissle 1917

To make chemically competent *E. coli* Nissle 1917 cells, bacteria were first grown to exponential phase by inoculating overnight culture in fresh LB broth at 1:100 dilution and incubated at 37 °C, 200 rpm for 2 h or until OD600 of 0.3 or 0.4 was reached. Cell culture at exponential phase was chilled on ice for 30 min. Followed by centrifugation at 3500 rpm, 4 °C for 10 min. The supernatant was removed, and the cells were washed twice with ice-cold $CaCl_2$ (0.1 M) and resuspended in $CaCl_2$(0.1 M) and glycerol (20% w/v).

For transformation, competent cells (100 μl) were added with a plasmid (100 ng) and mixed by flicking. The cell suspension was chilled on ice for 30 min and transferred to a 42 °C water bath for 45 seconds, followed by incubation on ice for 2 min. SOC media (900 μl) was added and mixed, and the cell suspension was incubated at 37 °C, 200 rpm for an hour before plating on kanamycin (60 μg/ml) agar plate.

Nitric oxide induction and time kinetics experiment

Transformed E. coli Nissle 1917 was first inoculated in a rich medium with supplemented antibiotics (Kanamycin 60 μg/ml; Carbenicillin 100 μg/ml) for 16 h 37 °C 250 rpm. For plate setup using EcN and *E. coli* DH5α, overnight culture with OD >1 was diluted 20 times (10 μl) and added to a final 200 μl plate reader induction volume (final OD 0.1~0.05). For plate setup using purified mini-SimCells, 100 μl of the purified filtrate (OD 0.1) was added with PBS to achieve a final 200 μl induction volume. To avoid any premature release of nitric oxide, a fresh

inducer stock was made from DETA/NO powder and dissolved in deionised water every time before induction. For kinetics reads, Tecan Spark was used to take sfGFP (Fixed gain = 80, exciting/emitting wavelength 480 nm/512 nm) measurement at a 15 min interval over the course of 16 h with inbuild kinetic function. Optical density at 600 nm was taken as reads for bacterial growth. The results were analysed and plotted using Prism software. Microscope images were taken using Olympus BX53 fluorescent microscope. Image analysis was performed using ImageJ to account for background correction.

Mini SimCell culturing and purification

Freshly transformed bacteria colony was picked into 2x concentrated LB medium (with no additional NaCl) and inoculated for 16 h at 37 °C 200 rpm, followed by centrifugation at 4000 g for 15 min to remove large cell pellets. Next, the supernatant (mini SimCell containing) was reinoculated with an antibiotic cocktail (Cefotaxime 100 μg/ml Ceftraxione 100 μg/ml and penicillin G sodium 100 μg/ml) for 1 hr at 37°C, 250 rpm to lyse any active growing parent cells. This was then put under 4°C overnight to eliminate any left-over or slow-growing progenitor cells. All centrifuge and liquid transfer procedures are kept at 4 °C or on ice to avoid any heat damage and prevent the energy loss by mini SimCells. Further separation of mini SimCell was done by gradient centrifugation (4000 g, 3000 g, 2000 g, and 1000 g) with 10 min interval using ultracentrifuge (Beckman Coulter Avanti JXN-26). The top and middle layers of the supernatant (2/3 of the liquid volume) were filtered using a 0.45 µm pore size mixed cellulose ester (MCE) ThermoFischer membrane for homogenisation purposes. The subsequent collection of mini SimCell was done using 0.22 µm pore size MCE membrane and resuspended in PBS with the antibiotic cocktail for further plate reader experiments. LB agar plates LB agar plate was made from LB broth with agar (Miller) and deionised water, together with added appropriate antibiotics (Kanamycin 50 µg/ml and Carbenicillin 100 µg/ml) were

used to check parent cell contamination (*E. coli ΔminD* MC1000 has chromosomal kanamycin marker remained and the plasmid confers carbenicillin/ampicillin resistance). The purified mini SimCells filtrate 100 µl was diluted 1 to 10^8 folds with PBS. Subsequently, 5 µl aliquots were plated onto a LB plate with three technical replicates. Aliquot plates were then incubated over 16 and 48 h, respectively, at 37°C to check for any sign of parent colony.

Counting of mini SimCells and parent cells

Mini SimCell and parents cell count was adopted from the formula used in [38],

$$N_{minicell} = OD_{600} \times 5 \times 10^{10}$$

$$N_{E.coli} = OD_{600} \times 7.8 \times 10^{10}$$

N represents the cell count per mL volume.

Freeze-drying protocol

Transformed cells were grown under optimal condition (LB, 37 °C 200 rpm) until they reach OD~0.4 – 0.5. then washed with PBS three times to remove any growth medium. Then resuspend with an equal volume of protection buffer (5% w/v BAS, 6% w/v Sucrose, 6% w/v Trehalose and 1.5% Dextran) and freeze in -80 °C overnight. Martin Christ Alpha 1- 4 LSC basic freeze drier was used for the lyophilisation process. The sample holder and inner chamber were prechilled to -20 °C to prevent any thawing. 0.1 mPa vacuum was applied for 12 h until all samples showed a light yellow colour. For bacteria revival, 1 ml of SOC medium was added to the dry powder and incubated for 15 min at 37 °C. Next, this was carried for plate reader induction. For induction experiments, a clear PBS medium was used instead to avoid the background masking.

Author contributions: W.E.H conceived original idea; X.J.C. and W.E.H. designed research; X.J.C. performed research; B.W. provided the norR mutant strains. B.W. and I.P.T. contributed new reagents/analytic tools; X.J.C. and W.E.H. analysed data; X.J.C. and W.E.H. wrote the paper, and all authors read and edited the manuscript.

Conflict of interest statement: Authors claim no conflict of interest of this work.

Acknowledgements

W.E.H. acknowledges support from EPSRC (EP/M002403/1 and EP/N009746/1). B.W. acknowledges support by the UK Research and Innovation Future Leaders Fellowship [MR/S018875/1], Leverhulme Trust research project grant [RPG-2020-241], US Office of Naval Research Global grant [N62909-20-1-2036].

Supplementary info

In silico model details and parameter used are provided in the supplementary info. Similarly, the sequence map and primer used for constructing each construct are also provided.

References

(1) Forbes, N. S. Engineering the Perfect (Bacterial) Cancer Therapy. *Nat. Rev. Cancer* **2010**, *10* (11), 785–794. https://doi.org/10.1038/nrc2934.

(2) Hwang, I. Y.; Tan, M. H.; Koh, E.; Ho, C. L.; Poh, C. L.; Chang, M. W. Reprogramming Microbes to Be Pathogen-Seeking Killers. *ACS Synth. Biol.* **2014**, *3* (4), 228–237. https://doi.org/10.1021/sb400077j.

(3) Din, M. O.; Danino, T.; Prindle, A.; Skalak, M.; Selimkhanov, J.; Allen, K.; Julio, E.; Atolia, E.; Tsimring, L. S.; Bhatia, S. N.; Hasty, J. Synchronized Cycles of Bacterial Lysis for in Vivo Delivery. *Nature* **2016**, *536* (7614), 81–85. https://doi.org/10.1038/nature18930.

(4) Leventhal, D. S.; Sokolovska, A.; Li, N.; Plescia, C.; Kolodziej, S. A.; Gallant, C. W.; Christmas, R.; Gao, J. R.; James, M. J.; Abin-Fuentes, A.; Momin, M.; Bergeron, C.; Fisher, A.; Miller, P. F.; West, K. A.; Lora, J. M. Immunotherapy with Engineered Bacteria by Targeting the STING Pathway for Anti-Tumor Immunity. *Nat. Commun.* **2020**, *11* (1), 1–15. https://doi.org/10.1038/s41467-020-16602-0.

(5) Ganai, S.; Arenas, R. B.; Forbes, N. S. Tumour-Targeted Delivery of TRAIL Using Salmonella Typhimurium Enhances Breast Cancer Survival in Mice. *Br. J. Cancer* **2009**, *101* (10), 1683–1691. https://doi.org/10.1038/sj.bjc.6605403.

(6) Chen, J. X.; Steel, H.; Wu, Y.-H.; Wang, Y.; Xu, J.; Rampley, C. P. N.; Thompson, I. P.; Papachristodoulou, A.; Huang, W. E. Characterisation and Development of Aspirin Inducible Biosensors in E. Coli and SimCells. *Appl. Environ. Microbiol.* **2019**, AEM.02959-18. https://doi.org/10.1128/AEM.02959-18.

(7) Bourdeau, R. W.; Lee-Gosselin, A.; Lakshmanan, A.; Farhadi, A.; Kumar, S. R.; Nety, S. P.; Shapiro, M. G. Acoustic Reporter Genes for Noninvasive Imaging of Microorganisms in Mammalian Hosts. *Nature* **2018**, *553* (7686), 86–90.

https://doi.org/10.1038/nature25021.

(8) McNerney, M. P.; Doiron, K. E.; Ng, T. L.; Chang, T. Z.; Silver, P. A. Theranostic Cells: Emerging Clinical Applications of Synthetic Biology. *Nat. Rev. Genet. 2021* **2021**, 1–17. https://doi.org/10.1038/s41576-021-00383-3.

(9) Kurtz, C. B.; Millet, Y. A.; Puurunen, M. K.; Perreault, M.; Charbonneau, M. R.; Isabella, V. M.; Kotula, J. W.; Antipov, E.; Dagon, Y.; Denney, W. S.; Wagner, D. A.; West, K. A.; Degar, A. J.; Brennan, A. M.; Miller, P. F. An Engineered E. Coli Nissle Improves Hyperammonemia and Survival in Mice and Shows Dose-Dependent Exposure in Healthy Humans. *Sci. Transl. Med.* **2019**, *11* (475), 7975. https://doi.org/10.1126/scitranslmed.aau7975.

(10) Courbet, A.; Endy, D.; Renard, E.; Molina, F.; Bonnet, J. Detection of Pathological Biomarkers in Human Clinical Samples via Amplifying Genetic Switches and Logic Gates. *Sci. Transl. Med.* **2015**, *7* (289), 83–89. https://doi.org/10.1126/scitranslmed.aaa3601.

(11) Maryadele, J. O. Neil. The Merck Index: An Encyclopedia of Chemicals, Drugs and Biologicals. Merck and Co. *Inc. Whitehouse Station. New Jersey* **2006**, p1131. https://doi.org/https://doi.org/10.1002/ddr.21085.

(12) Valko, M.; Leibfritz, D.; Moncol, J.; Cronin, M. T. D.; Mazur, M.; Telser, J. Free Radicals and Antioxidants in Normal Physiological Functions and Human Disease. *International Journal of Biochemistry and Cell Biology*. Pergamon January 1, 2007, pp 44–84. https://doi.org/10.1016/j.biocel.2006.07.001.

(13) Avdagić, N.; Zaćiragić, A.; Babić, N.; Hukić, M.; Šeremet, M.; Lepara, O.; Nakaš-Ićindić, E. Nitric Oxide as a Potential Biomarker in Infl Ammatory Bowel Disease. *Bosn. J. Basic Med. Sci.* **2013**, *13* (1), 5–9. https://doi.org/10.17305/bjbms.2013.2402.

(14) Korde Choudhari, S.; Chaudhary, M.; Bagde, S.; Gadbail, A. R.; Joshi, V. Nitric Oxide

and Cancer: A Review. *World Journal of Surgical Oncology*. BioMed Central May 30, 2013, p 118. https://doi.org/10.1186/1477-7819-11-118.

(15) Barbato, J. E.; Tzeng, E. Nitric Oxide and Arterial Disease. *Journal of Vascular Surgery*. Mosby July 1, 2004, pp 187–193. https://doi.org/10.1016/j.jvs.2004.03.043.

(16) Seth, P.; Hsieh, P. N.; Jamal, S.; Wang, L.; Gygi, S. P.; Jain, M. K.; Coller, J.; Stamler, J. S. Regulation of MicroRNA Machinery and Development by Interspecies S-Nitrosylation. *Cell* **2019**, *176* (5), 1014-1025.e12. https://doi.org/10.1016/j.cell.2019.01.037.

(17) Tucker, N. P.; D'Autréaux, B.; Studholme, D. J.; Spiro, S.; Dixon, R. DNA Binding Activity of the Escherichia Coli Nitric Oxide Sensor NorR Suggests a Conserved Target Sequence in Diverse Proteobacteria. *J. Bacteriol.* **2004**, *186* (19), 6656–6660. https://doi.org/10.1128/JB.186.19.6656-6660.2004.

(18) Rodionov, D. A.; Dubchak, I. L.; Arkin, A. P.; Alm, E. J.; Gelfand, M. S. Dissimilatory Metabolism of Nitrogen Oxides in Bacteria: Comparative Reconstruction of Transcriptional Networks. *PLoS Comput. Biol.* **2005**, *1* (5), 0415–0431. https://doi.org/10.1371 /journal.pcbi.001 OOS5.

(19) Tucker, N. P.; Ghosh, T.; Bush, M.; Zhang, X.; Dixon, R. Essential Roles of Three Enhancer Sites in Σ54-Dependent Transcription by the Nitric Oxide Sensing Regulatory Protein NorR. *Nucleic Acids Res.* **2009**, *38* (4), 1182–1194. https://doi.org/10.1093/nar/gkp1065.

(20) Gardner, A. M.; Gessner, C. R.; Gardner, P. R. Regulation of the Nitric Oxide Reduction Operon (NorRVW) in Escherichia Coli. Role of NorR and Σ54 in the Nitric Oxide Stress Response. *J. Biol. Chem.* **2003**, *278* (12), 10081–10086. https://doi.org/10.1074/jbc.M212462200.

(21) Archer, E. J.; Robinson, A. B.; Süel, G. M. Engineered E. Coli That Detect and Respond

to Gut Inflammation through Nitric Oxide Sensing. *ACS Synth. Biol.* **2012**, *1* (10), 451–457. https://doi.org/10.1021/sb3000595.

(22) Tucker, N.; D'Autréaux, B.; Spiro, S.; Dixon, R. DNA Binding Properties of the Escherichia Coli Nitric Oxide Sensor NorR: Towards an Understanding of the Regulation of Flavorubredoxin Expression. In *Biochemical Society Transactions*; Portland Press, 2005; Vol. 33, pp 181–183. https://doi.org/10.1042/BST0330181.

(23) Büsch, A.; Pohlmann, A.; Friedrich, B.; Cramm, R. A DNA Region Recognized by the Nitric Oxide-Responsive Transcriptional Activator NorR Is Conserved in β and γ-Proteobacteria. *J. Bacteriol.* **2004**, *186* (23), 7980–7987. https://doi.org/10.1128/JB.186.23.7980-7987.2004.

(24) D'Autréaux, B.; Tucker, N.; Spiro, S.; Dixon, R. Characterization of the Nitric Oxide-Reactive Transcriptional Activator NorR. *Methods in Enzymology*. 2008, pp 235–251. https://doi.org/10.1016/S0076-6879(07)37013-4.

(25) D'Autréaux, B.; Tucker, N. P.; Dixon, R.; Spiro, S. A Non-Haem Iron Centre in the Transcription Factor NorR Senses Nitric Oxide. *Nature* **2005**, *437* (7059), 769–772. https://doi.org/10.1038/nature03953.

(26) Tucker, N. P.; D'Autréaux, B.; Spiro, S.; Dixon, R. Mechanism of Transcriptional Regulation by the Escherichia Coli Nitric Oxide Sensor NorR. In *Biochemical Society transactions*; 2006; Vol. 34, pp 191–194. https://doi.org/10.1042/BST0340191.

(27) Davis, J. H.; Rubin, A. J.; Sauer, R. T. Design, Construction and Characterization of a Set of Insulated Bacterial Promoters. *Nucleic Acids Res.* **2011**, *39* (3), 1131–1141. https://doi.org/10.1093/nar/gkq810.

(28) Mokry, R. L.; Schumacher, M. L.; Hogg, N.; Terhune, S. S. Nitric Oxide Circumvents Virus-Mediated Metabolic Regulation during Human Cytomegalovirus Infection. *MBio* **2020**, *11* (6), 1–25. https://doi.org/10.1128/mBio.02630-20.

(29) Willardson, B. M.; Wilkins, J. F.; Rand, T. A.; Schupp, J. M.; Hill, K. K.; Keim, P.; Jackson, P. J. Development and Testing of a Bacterial Biosensor for Toluene-Based Environmental Contaminants. *Appl. Environ. Microbiol.* **1998**, *64* (3), 1006–1012. https://doi.org/10.1128/aem.64.3.1006-1012.1998.

(30) Huang, W. E.; Singer, A. C.; Spiers, A. J.; Preston, G. M.; Whiteley, A. S. Characterizing the Regulation of the Pu Promoter in Acinetobacter Baylyi ADP1. *Environ. Microbiol.* **2008**, *10*, 1668–1680. https://doi.org/10.1111/j.1462-2920.2008.01583.x.

(31) Jovanovic, M.; James, E. H.; Burrows, P. C.; Rego, F. G. M.; Buck, M.; Schumacher, J. Regulation of the Co-Evolved HrpR and HrpS AAA+ Proteins Required for Pseudomonas Syringae Pathogenicity. *Nat. Commun.* **2011**, *2* (1), 1–9. https://doi.org/10.1038/ncomms1177.

(32) Chen, J. X.; Steel, H.; Wu, Y. H.; Wang, Y.; Xu, J.; Rampley, C. P. N.; Thompson, I. P.; Papachristodoulou, A.; Huang, W. E. Development of Aspirininducible Biosensors in Escherichia Coli and SimCells. *Appl. Environ. Microbiol.* **2019**, *85* (6), 2959–2977. https://doi.org/10.1128/AEM.02959-18.

(33) Freundlich, M.; Ramani, N.; Mathew, E.; Sirko, A.; Tsui, P. *The Role of Integration Host Factor In Gene Expression in Escherichia Coli*; John Wiley & Sons, Ltd, 1992; Vol. 6, pp 2557–2563. https://doi.org/10.1111/j.1365-2958.1992.tb01432.x.

(34) Huo, Y. X.; Zhang, Y. T.; Xiao, Y.; Zhang, X.; Buck, M.; Kolb, A.; Wang, Y. P. IHF-Binding Sites Inhibit DNA Loop Formation and Transcription Initiation. *Nucleic Acids Res.* **2009**, *37* (12), 3878–3886. https://doi.org/10.1093/nar/gkp258.

(35) Justino, M. C.; Gonçalves, V. M. M.; Saraiva, L. M. Binding of NorR to Three DNA Sites Is Essential for Promoter Activation of the Flavorubredoxin Gene, the Nitric Oxide Reductase of Escherichia Coli. *Biochem. Biophys. Res. Commun.* **2005**, *328* (2), 540–

544. https://doi.org/10.1016/j.bbrc.2005.01.008.

(36) Sonnenborn, U.; Schulze, J. The Non-Pathogenic Escherichia Coli Strain Nissle 1917- Features of a Versatile Probiotic. *Microb. Ecol. Health Dis.* **2009**, *21* (3–4), 122–158. https://doi.org/http://dx.doi.org/10.3109/08910600903444267.

(37) Rampley, C. P. N.; Davison, P. A.; Qian, P.; Preston, G. M.; Hunter, C. N.; Thompson, I. P.; Wu, L. J.; Huang, W. E. Development of SimCells as a Novel Chassis for Functional Biosensors. *Sci. Rep.* **2017**, *7* (1), 7261. https://doi.org/10.1038/s41598-017-07391-6.

(38) Jivrajani, M.; Shrivastava, N.; Nivsarkar, M. A Combination Approach for Rapid and High Yielding Purification of Bacterial Minicells. *J. Microbiol. Methods* **2013**, *92* (3), 340–343. https://doi.org/10.1016/j.mimet.2012.12.002.

(39) MacDiarmid, J. A.; Mugridge, N. B.; Weiss, J. C.; Phillips, L.; Burn, A. L.; Paulin, R. P. P.; Haasdyk, J. E.; Dickson, K. A.; Brahmbhatt, V. N.; Pattison, S. T.; James, A. C.; Al Bakri, G.; Straw, R. C.; Stillman, B.; Graham, R. M.; Brahmbhatt, H. Bacterially Derived 400 Nm Particles for Encapsulation and Cancer Cell Targeting of Chemotherapeutics. *Cancer Cell* **2007**, *11* (5), 431–445. https://doi.org/10.1016/j.ccr.2007.03.012.

(40) Francke, C.; Groot Kormelink, T.; Hagemeijer, Y.; Overmars, L.; Sluijter, V.; Moezelaar, R.; Siezen, R. J. Comparative Analyses Imply That the Enigmatic Sigma Factor 54 Is a Central Controller of the Bacterial Exterior. *BMC Genomics* **2011**, *12* (1), 1–21. https://doi.org/10.1186/1471-2164-12-385.

(41) Brown, D. R.; Barton, G.; Pan, Z.; Buck, M.; Wigneshweraraj, S. Nitrogen Stress Response and Stringent Response Are Coupled in Escherichia Coli. *Nat. Commun.* **2014**, *5* (1), 1–8. https://doi.org/10.1038/ncomms5115.

(42) Guttenplan, S. B.; Kearns, D. B. Regulation of Flagellar Motility during Biofilm

Formation. *FEMS Microbiology Reviews*. NIH Public Access November 2013, pp 849–871. https://doi.org/10.1111/1574-6976.12018.

(43) Reitzer, L.; Schneider, B. L. Metabolic Context and Possible Physiological Themes of 54-Dependent Genes in Escherichia Coli. *Microbiol. Mol. Biol. Rev.* **2001**, *65* (3), 422–444. https://doi.org/10.1128/mmbr.65.3.422-444.2001.

(44) Jishage, M.; Iwata, A.; Ueda, S.; Ishihama, A. Regulation of RNA Polymerase Sigma Subunit Synthesis in Escherichia Coli: Intracellular Levels of Four Species of Sigma Subunit under Various Growth Conditions. *J. Bacteriol.* **1996**, *178* (18), 5447–5451. https://doi.org/10.1128/jb.178.18.5447-5451.1996.

(45) Ishihama, A. Functional Modulation of Escherichia Coli RNA Polymerase. *Annual Review of Microbiology*. Annual Reviews 4139 El Camino Way, P.O. Box 10139, Palo Alto, CA 94303-0139, USA November 28, 2000, pp 499–518. https://doi.org/10.1146/annurev.micro.54.1.499.

(46) Gui, Q.; Lawson, T.; Shan, S.; Yan, L.; Liu, Y. *The Application of Whole Cell-Based Biosensors for Use in Environmental Analysis and in Medical Diagnostics*; MDPI AG, 2017; Vol. 17, p 1623. https://doi.org/10.3390/s17071623.

(47) Bush, M.; Dixon, R. The Role of Bacterial Enhancer Binding Proteins as Specialized Activators of 54-Dependent Transcription. *Microbiol. Mol. Biol. Rev.* **2012**, *76* (3), 497–529. https://doi.org/10.1128/mmbr.00006-12.

(48) Rosenfeld, N.; Elowitz, M. B.; Alon, U. Negative Autoregulation Speeds the Response Times of Transcription Networks. *J. Mol. Biol.* **2002**, *323* (5), 785–793. https://doi.org/10.1016/S0022-2836(02)00994-4.

(49) Wang, B.; Barahona, M.; Buck, M. Amplification of Small Molecule-Inducible Gene Expression via Tuning of Intracellular Receptor Densities. *Nucleic Acids Res.* **2015**, *43* (3), 1955–1964. https://doi.org/10.1093/nar/gku1388.

(50) Robinson, J. L.; Brynildsen, M. P. A Kinetic Platform to Determine the Fate of Nitric Oxide in Escherichia Coli. *PLoS Comput. Biol.* **2013**, *9* (5), e1003049. https://doi.org/10.1371/journal.pcbi.1003049.

(51) Meng, Q.; Yin, J.; Jin, M.; Gao, H. Distinct Nitrite and Nitric Oxide Physiologies in Escherichia Coli and Shewanella Oneidensis. *Appl. Environ. Microbiol.* **2018**, *84* (12). https://doi.org/10.1128/AEM.00559-18.

(52) Ridnour, L. A.; Isenberg, J. S.; Espey, M. G.; Thomas, D. D.; Roberts, D. D.; Wink, D. A. Nitric Oxide Regulates Angiogenesis through a Functional Switch Involving Thrombospondin-1. *Proc. Natl. Acad. Sci.* **2005**, *102* (37), 13147–13152. https://doi.org/10.1073/PNAS.0502979102.

(53) Vahora, H.; Khan, M. A.; Alalami, U.; Hussain, A. The Potential Role of Nitric Oxide in Halting Cancer Progression Through Chemoprevention. *J. Cancer Prev.* **2016**, *21* (1), 1–12. https://doi.org/10.15430/jcp.2016.21.1.1.

(54) Williams, D. E.; Nisbett, L. M.; Bacon, B.; Boon, E. Bacterial Heme-Based Sensors of Nitric Oxide. *Antioxidants and Redox Signaling*. Mary Ann Liebert Inc. December 20, 2018, pp 1872–1887. https://doi.org/10.1089/ars.2017.7235.

(55) Burke, A. J.; Sullivan, F. J.; Giles, F. J.; Glynn, S. A. The Yin and Yang of Nitric Oxide in Cancer Progression. *Carcinogenesis* **2013**, *34* (3), 503–512. https://doi.org/10.1093/CARCIN/BGT034.

(56) Iverson, N. M.; Hofferber, E. M.; Stapleton, J. A. Nitric Oxide Sensors for Biological Applications. *Chemosens. 2018, Vol. 6, Page 8* **2018**, *6* (1), 8. https://doi.org/10.3390/CHEMOSENSORS6010008.

(57) Ding, Y.; Gardiner, D. M.; Xiao, D.; Kazan, K. Regulators of Nitric Oxide Signaling Triggered by Host Perception in a Plant Pathogen. *Proc. Natl. Acad. Sci. U. S. A.* **2020**, *117* (20), 11147–11157. https://doi.org/10.1073/pnas.1918977117.

(58) Gu, D.; Zhang, Y.; Wang, Q.; Zhou, X. S-Nitrosylation-Mediated Activation of a Histidine Kinase Represses the Type 3 Secretion System and Promotes Virulence of an Enteric Pathogen. *Nat. Commun.* **2020**, *11* (1), 1–19. https://doi.org/10.1038/s41467-020-19506-1.

(59) Westendorf, A. M.; Gunzer, F.; Deppenmeier, S.; Tapadar, D.; Hunger, J. K.; Schmidt, M. A.; Buer, J.; Bruder, D. Intestinal Immunity of Escherichia Coli NISSLE 1917: A Safe Carrier for Therapeutic Molecules. *FEMS Immunol. Med. Microbiol.* **2005**, *43* (3), 373–384. https://doi.org/10.1016/J.FEMSIM.2004.10.023.

(60) Bourdeau, R. W.; Lee-Gosselin, A.; Lakshmanan, A.; Farhadi, A.; Kumar, S. R.; Nety, S. P.; Shapiro, M. G. Acoustic Reporter Genes for Noninvasive Imaging of Microbes in Mammalian Hosts. *Nature* **2018**, *553* (7686), 86. https://doi.org/10.1038/NATURE25021.

(61) Riglar, D. T.; Richmond, D. L.; Potvin-Trottier, L.; Verdegaal, A. A.; Naydich, A. D.; Bakshi, S.; Leoncini, E.; Lyon, L. G.; Paulsson, J.; Silver, P. A. Bacterial Variability in the Mammalian Gut Captured by a Single-Cell Synthetic Oscillator. *Nat. Commun.* **2019**, *10* (1). https://doi.org/10.1038/s41467-019-12638-z.

(62) Daeffler, K. N.-M. N.; Galley, J. D.; Sheth, R. U.; Ortiz-Velez, L. C.; Bibb, C. O.; Shroyer, N. F.; Britton, R. A.; Tabor, J. J.; Ortiz-Velez, L. C.; Bibb, C. O.; Shroyer, N. F.; Britton, R. A.; Tabor, J. J. Engineering Bacterial Thiosulfate and Tetrathionate Sensors for Detecting Gut Inflammation. *Mol. Syst. Biol.* **2017**, *13* (4), 923. https://doi.org/10.15252/msb.20167416.

(63) Cases, I.; De Lorenzo, V. V.; Perez-Martin, J.; Pérez-Martín, J. Involvement of Σ54 in Exponential Silencing of the Pseudomonas Putida TOL Plasmid Pu Promoter. *Mol. Microbiol.* **1996**, *19* (1), 7–17. https://doi.org/10.1046/j.1365-2958.1996.345873.x.

(64) Cases, I.; de Lorenzo, V. Promoters in the Environment: Transcriptional Regulation in

Its Natural Context. *Nature Reviews Microbiology*. Nature Publishing Group February 2005, pp 105–118. https://doi.org/10.1038/nrmicro1084.

(65) Atkinson, M. R.; Blauwkamp, T. A.; Bondarenko, V.; Studitsky, V.; Ninfa, A. J. Activation of the GlnA, GlnK, and Nac Promoters as Escherichia Coli Undergoes the Transition from Nitrogen Excess Growth to Nitrogen Starvation. *J. Bacteriol.* **2002**, *184* (19), 5358–5363. https://doi.org/10.1128/JB.184.19.5358-5363.2002.

(66) Carmona, M.; Fernández, S.; Rodríguez, M. J.; De Lorenzo, V. M-Xylene-Responsive Pu-PnifH Hybrid Σ54 Promoters That Overcome Physiological Control in Pseudomonas Putida KT2442. *J. Bacteriol.* **2005**, *187* (1), 125–134. https://doi.org/10.1128/JB.187.1.125-134.2005.

(67) Carmona, M.; De Lorenzo, V.; Bertoni, G. Recruitment of RNA Polymerase Is a Rate-Limiting Step for the Activation of the Σ54 Promoter Pu of Pseudomonas Putida. *J. Biol. Chem.* **1999**, *274* (47), 33790–33794. https://doi.org/10.1074/jbc.274.47.33790.

(68) Kan, A.; Gelfat, I.; Emani, S.; Praveschotinunt, P.; Joshi, N. S. Plasmid Vectors for in Vivo Selection-Free Use with the Probiotic *E. coli* Nissle 1917. *ACS Synth. Biol.* **2020**, *10* (1), 94–106. https://doi.org/10.1021/ACSSYNBIO.0C00466.

(69) Fan C., Davison P.A., Habgood R., Zeng H., Decker C.M., Gesell-Salazar M., Lueangwattanapong K., Townley H.E., Yang A., Thompson I.P., Ye H., Cui Z,. Schmidt F., Hunter C.N., Huang WE. Chromosome-free bacterial cells are safe and programmable platforms for synthetic biology (2020) *Proc Natl Acad Sci U S A.* 117: 6752–6761. https:// doi: 10.1073/pnas.1918859117.

(70) Takahashi, M. K.; Tan, X.; Dy, A. J.; Braff, D.; Akana, R. T.; Furuta, Y.; Donghia, N.; Ananthakrishnan, A.; Collins, J. J. A Low-Cost Paper-Based Synthetic Biology Platform for Analyzing Gut Microbiota and Host Biomarkers. *Nat. Commun. 2018 91* **2018**, *9* (1), 1–12. https://doi.org/10.1038/s41467-018-05864-4.

(71) Datsenko, K. A.; Wanner, B. L. One-Step Inactivation of Chromosomal Genes in Escherichia Coli K-12 Using PCR Products. *Proc. Natl. Acad. Sci. U. S. A.* **2000**, *97* (12), 6640–6645. https://doi.org/10.1073/pnas.120163297.

Table 1. Strains and plasmids used in this study

Strains	Genotype	Ref
E. coli K12 Δ*n*orR	*F′proA+B+ lacIq Δ(lacZ)M15 zzf::Tn10(TetR)/ fhuA2 glnV Δ(lac-proAB) thi-1 Δ(hsdS-mcrB)5 ΔnorR*	this study
E. coli Nissle 1917	*Ardeypharm GmbH*	-
E. coli DH5α	*fhuA2 Δ(argF-lacZ)U169 phoA glnV44 Φ80 Δ(lacZ)M15 gyrA96 recA1 relA1 endA1 thi-1 hsdR17*	NEB
E. coli MC1000 ΔminD	*F– λ– Δ(ara-leu)7697 [araD139]B/r Δ(codB-lacI)3 galK16 galE15 e14– mcrA0 relA1 rpsL150(StrR) spoT1 mcrB1 hsdR2(r–m+) Δ miniD:kanR*	37

Short abbreviations	Description	Ori	Ref
pPnorV	pGEMT_P_{norV}_ sfGFP_norR with wild type P_{norV}	ColE1	this study
pPnorVβ	pGEMT_P_{norV}_Beta_sfGFP_norR, P_{norV}_sfGFP_norR with single IHF site promoter $P_{norVβ}$	ColE1	this study
pPnorVnull	pGEMT_P_{norV_null}_sfGFP_norR, P_{norV}_sfGFP_norR with deleted IHFs site promoter $PnorV_{null}$	ColE1	this study
pProA	pGEMT_P_{roA}_norR_PnorV_sfGFP, *norR* orf under control of constitutive promoter P_{roA}, no feedback.	ColE1	this study
pProC	pGEMT_P_{roC}_norR_PnorV_sfGFP, *norR* orf under control of constitutive promoter P_{roC}, no feedback.	ColE1	this study
pProD	pGEMT_P_{roD}_norR_PnorV_sfGFP, *norR* orf under control of constitutive promoter P_{roD}, no feedback.	ColE1	this study

803 **Table 3.** Dynamic property of characterised NorR-based sensor circuit in this study.

Short abberivations	Circuits Name	Dynamic range (RFU)	Operational range (DETA/NO μM)	Limitation of detection (DETA/NO μM)	Strains tested	Response time (min)
pPnorVnull	$pP_{norVnull}$-sfGFP-norR	2989±128—5540±172	1000~2000	1000	*E. coli* Nissle 1917	~60
pPnorV	pP_{norV}-sfGFP-norR	2847±36--13931±193	1.5~500	1.5	*E. coli* Nissle 1917	~25
pPnorVβ	p $P_{norV\beta}$ -sfGFP-norR	3118±35--20762±2326	1.5~500	1.5	*E. coli* Nissle 1917/ DH5α	~25
pProD	pP_{roD}-norR-PnorV-sfGFP	1847±8--2257±79	1.5~500	1.5	*E. coli* Nissle 1917	~25
pProC	pP_{roC}-norR-PnorV-sfGFP	1728±59--3465±136	1.5~500	1.5	*E. coli* Nissle 1917	~25
pProA	pP_{roA}-norR-PnorV-sfGFP	1614±82--8220± 816	1.5~500	1.5	*E. coli* Nissle 1917	~25

804

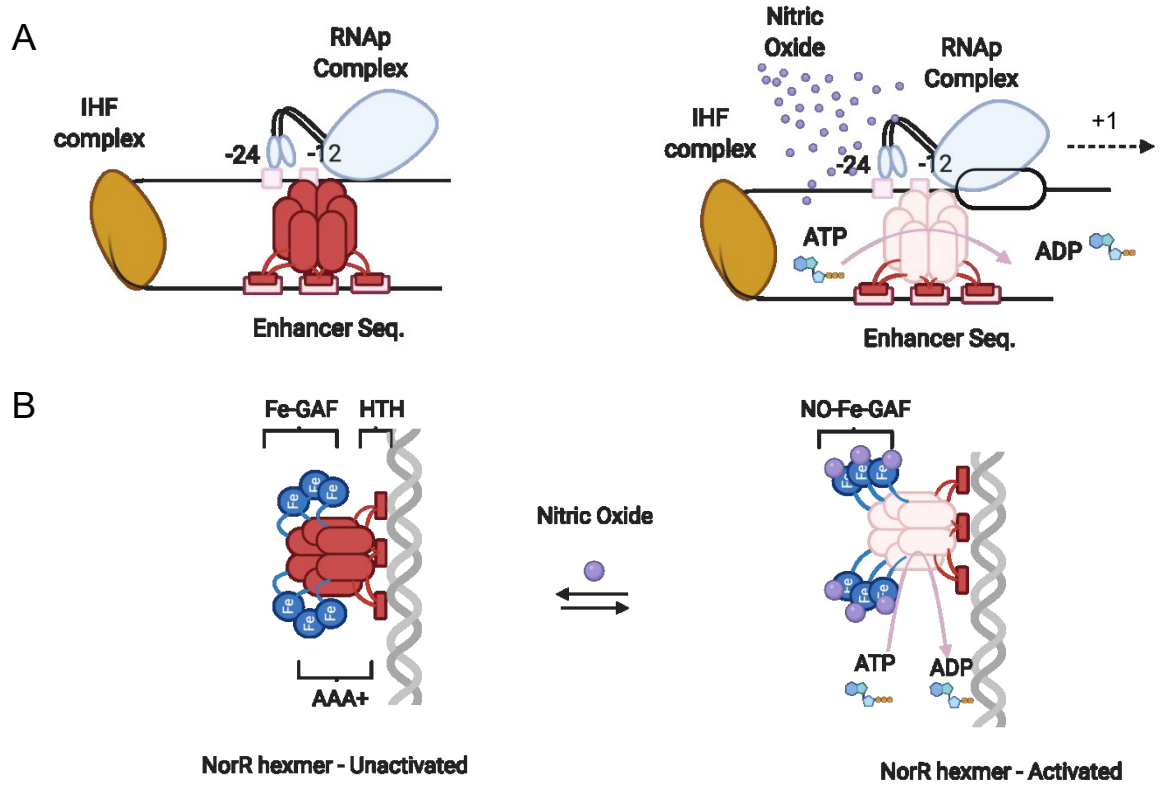

Figure 1. Molecular mechanism of NorR mediated σ54 dependent transcriptional activation. A) P_{NorV} promoter in its off state. Integration host factors (Yellow) bends DNA with a near 160° sharp angle to allow NorR (Red) homohexamer contact with $\boldsymbol{\sigma}^{54}$ factor at its binding site (-24) & (-12). NorR binding with upstream enhancer sequence are showed in pink block. In the absence of inducer, RNAp complex is closed from transcription. Upon nitric oxide binding, NorR exposes its AAA+ ATPase domain and activate $\boldsymbol{\sigma}^{54}$ into its active form for DNA opening and transcriptional initiation. B) The way NorR interacts with nitric oxides is through its non-haem iron center (Blue), which signals a reversible conformation change that opens up the ATPase domain upon binding.

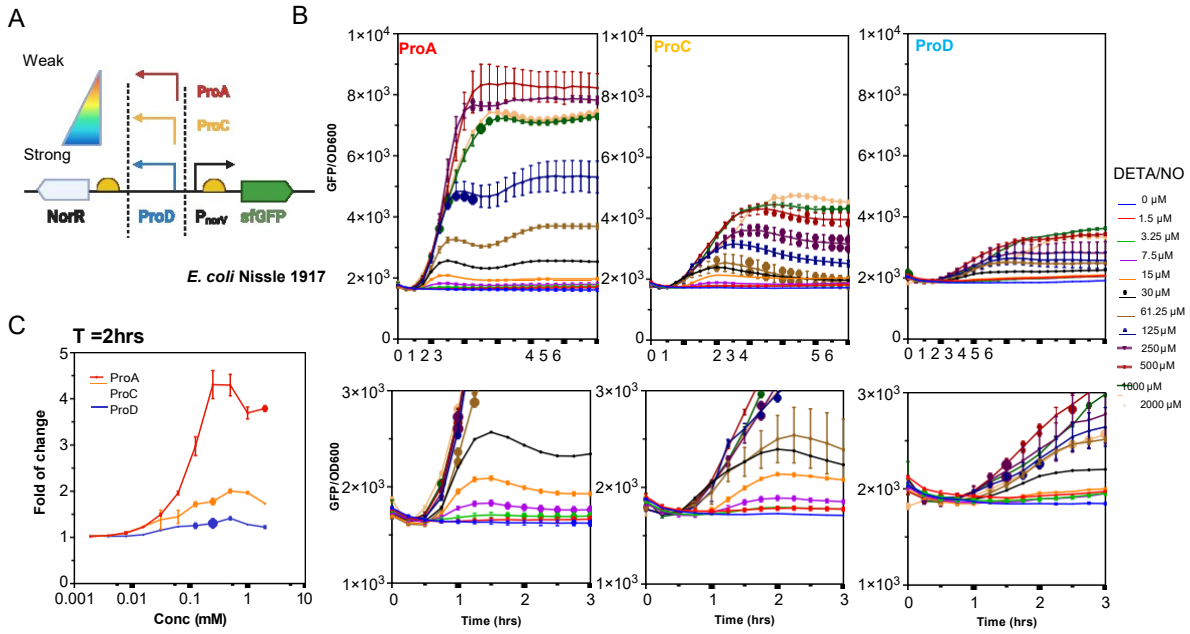

Figure 2. Performance of NO responsive circuits in open loop format with different promoter. A) Schematic diagram for the open loop sensor circuit with constitutive promoters of different strengths. B) Dynamical behaviors of induced gene circuits within 6 h. The first 3h was magnified to indicate the limit of detection. DETA/NO gradient used is (0, 1.5, 3.25, 7.5, 15, 30, 61.25, 125, 250, 500, 1000, 2000 μM) C) Fold of change curve of each constructs at T=2 hrs (steady state). Three biological replicates were tested. Error bars, s.d. (n=3).

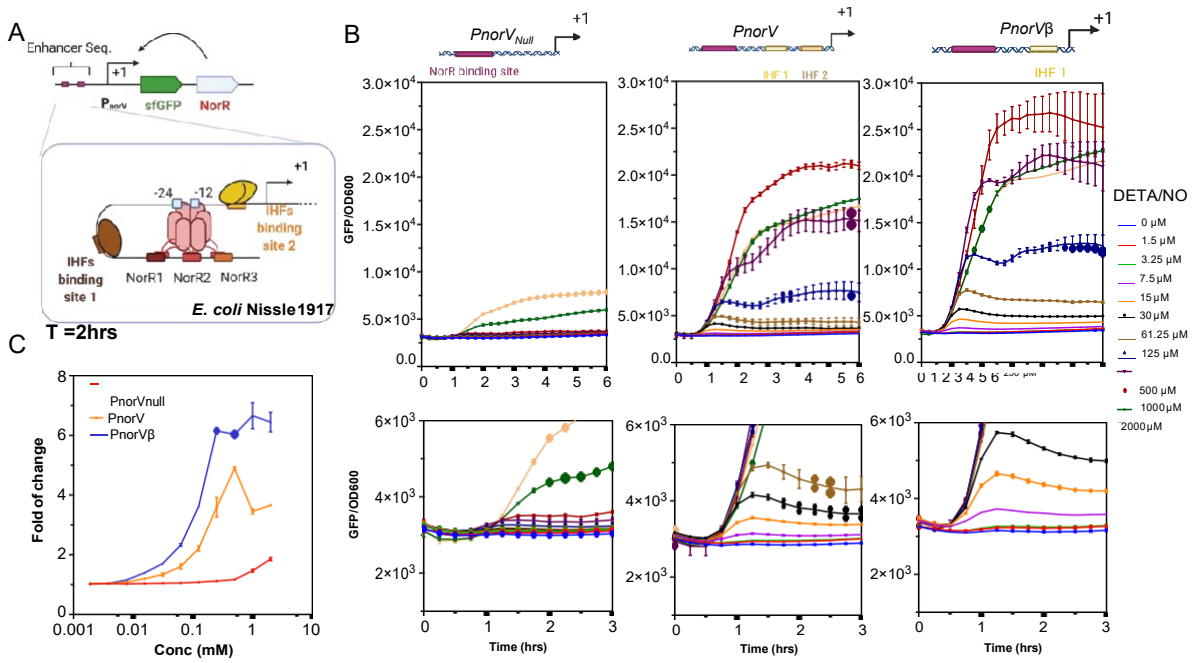

Figure 3. Performance of NO sensor with positive feedback design and the effect of IHF spacers. A) Schematic diagram of modified construct in positive feedback format. The PnorV promoter annotation with two IHFs sites and NorR binding site were shown in box. B) System induction kinetics (6 h) and the first 3h was magnified to show the limit of detection for each circuit. DETA/NO gradient used is (0, 1.5, 3.25, 7.5, 15, 30, 61.25, 125, 250, 500, 1000, 2000 μM) C) Fold of change for each circuit at T=2 h (Steady state). Three biological replicates were tested. Error bars, s.d. (n=3).

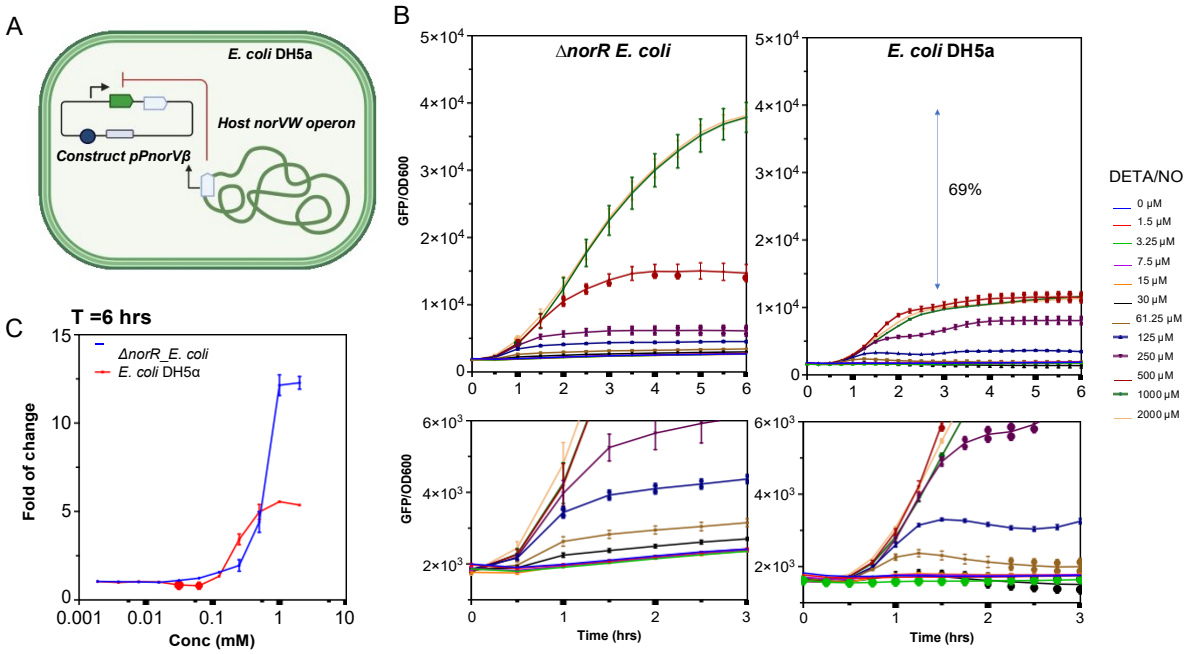

Figure 4. Host interference and sensor circuits' performance in *E. coli* Δ*norR* strain. A) Graphical representation of the potential impact of endogenous copy of NorR. B) System induction (6 h) dynamics in both *E. coli* DH5α and *E. coli* DH5α ΔnorR. The first 3h was magnified to indicate the limit of detection DETA/NO gradient used is (0, 1.5, 3.25, 7.5, 15, 30, 61.25, 125, 250, 500, 1000, 2000 μM). C) Fold of change curve at the steady state (T=2 h). Three biological replicates were tested. Error bars, s.d. (n=3).

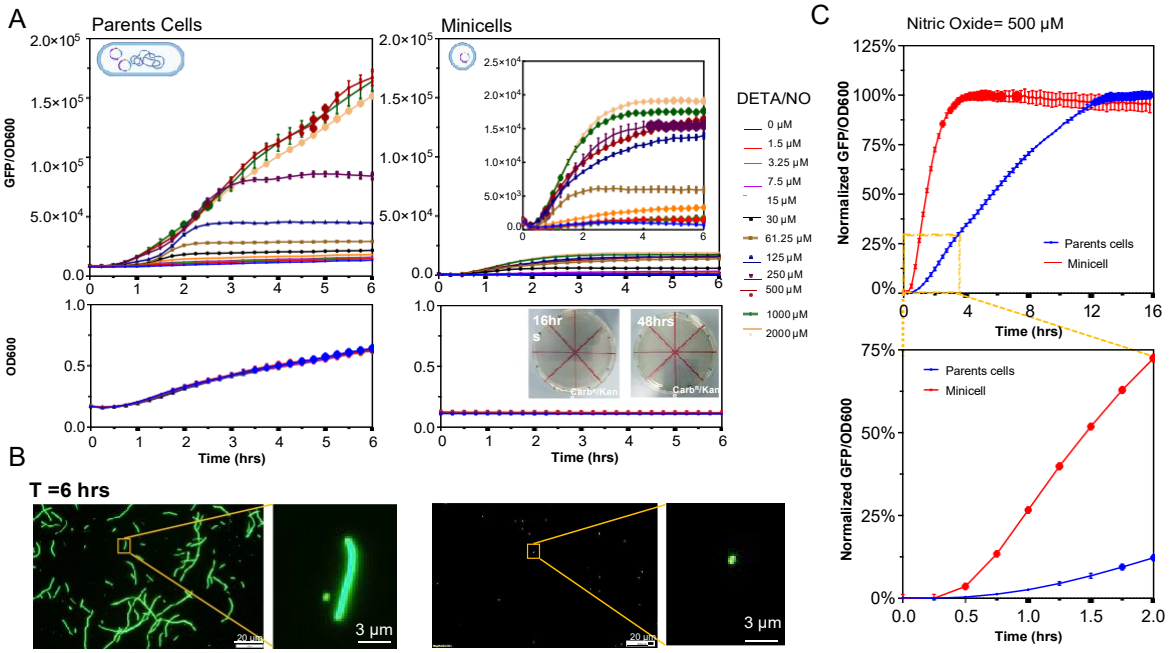

Figure 5. Optimised NO sensor (p PnorVβ**) is functional in mini SimCells.** A) NorR system induction kinetics of parent cells and mini SimCells with varying DETA/NO inductions (0, 1.5, 3.25, 7.5, 15, 30, 61.25, 125, 250, 500, 1000 µM). OD growth and plate assays (16 h and 48 h) were shown to indicate any parent cell contamination in the mini SimCell pool. Microscope images taken to indicate the relative size of mini SimCells compared to parent cells. Scale bar = 20 µm and enlarged Figures with scale bar = 3 µm. B) Normalized induction kinetics for parent cells and mini SimCells under 500 µM (saturated concentration). C) Relative fluorescence reads were normalised against the highest reads and shown as percentage to compare the response time and lagging time between two systems. First 2h was enlarged and shown on the bottom. Three biological replicates were tested. Error bars, s.d. (*n*=3).

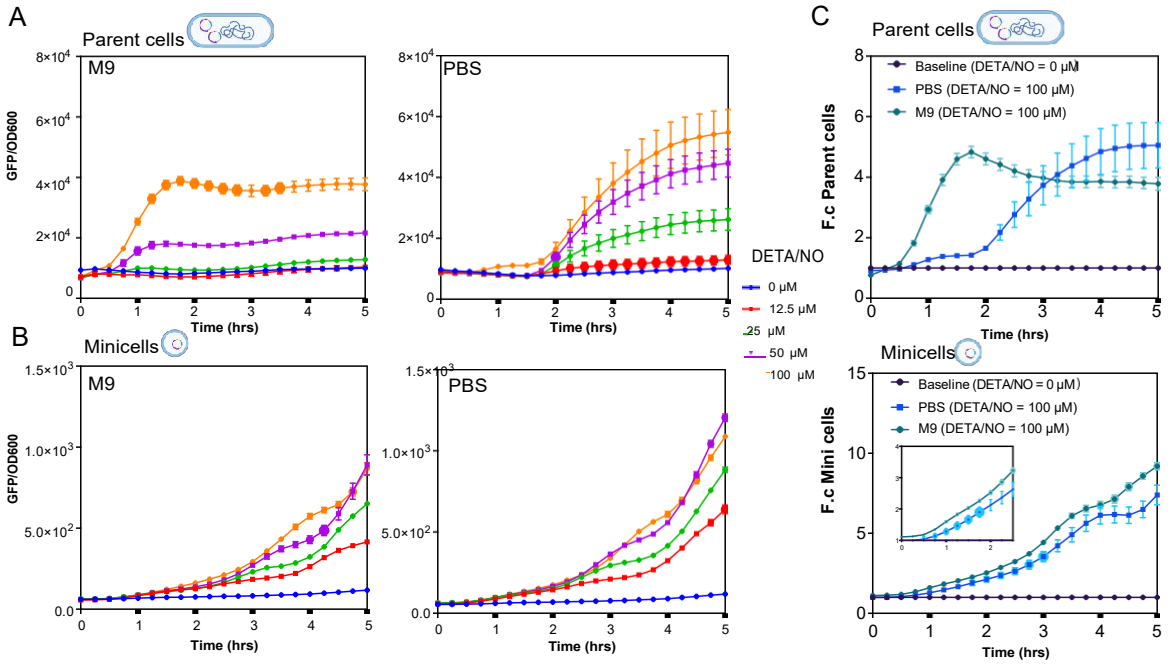

Figure 6. Mini SimCell-based NO sensor bypassed host interference. A) Induction kinetics of pPnorVβ circuits function in *E. coli* MC1000 ΔMinD under nitrogen depleted condition (PBS) or nitrogen supplied condition M9 condition. Each medium condition was supplemented with 2% w/v glycerol as carbon source. B) Induction kinetics of the purified mini SimCells loaded with the same construct. DETA/NO gradient used is (0, 12.5, 25, 50, 100 μM). C)Fold of induction changes in both cases. (GFP fully induced/ GFP uninduced). The first 1h of minicell induction was enlarged and shown in subplot. Three biological replicates were tested. Error bars, s.d. (n=3).

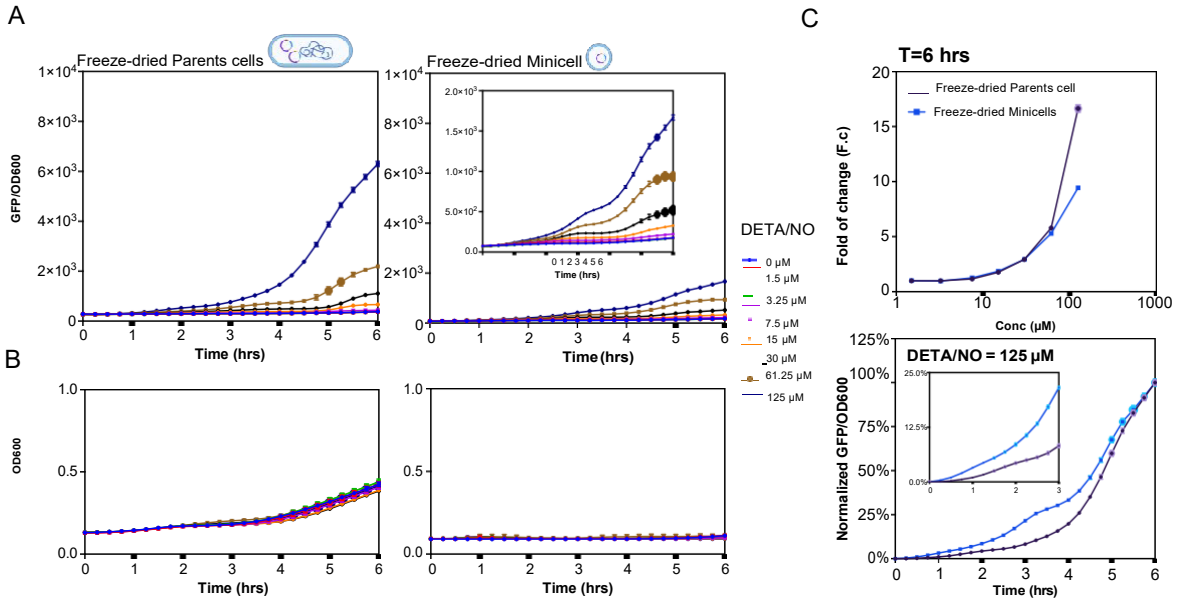

Figure 7. Freeze-dried mini SimCells retained sensor function over two-months. A) Parent cell (*E. coli* MC1000 Δ*minD*) and mini SimCells were transformed with optimised nitric oxide sensing circuits (pPnorVβ) and carried out the lyophilization process. After two-month storage in room temperature (25 ºC). Cells were revived using SOC medium and tested for induction performance. DETA/NO gradient used here is (0, 1.5, 3.25, 7.5, 15, 30, 61.25, 125 µM). B) OD at 600 nm was also recorded to indicate no parent cell contamination. C) Fold of inductions were shown for both cases, percentage of induction was shown to compare the system response speed, first 3h was enlarged in subplot. Three biological replicates were tested. Error bars, s.d. (n = 3).

Graphic Abstract:

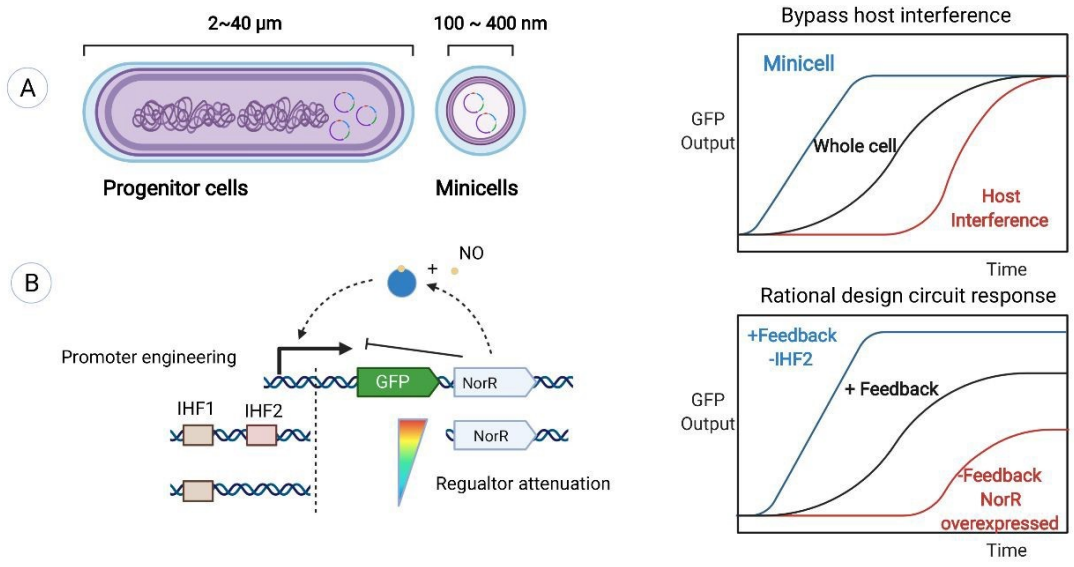

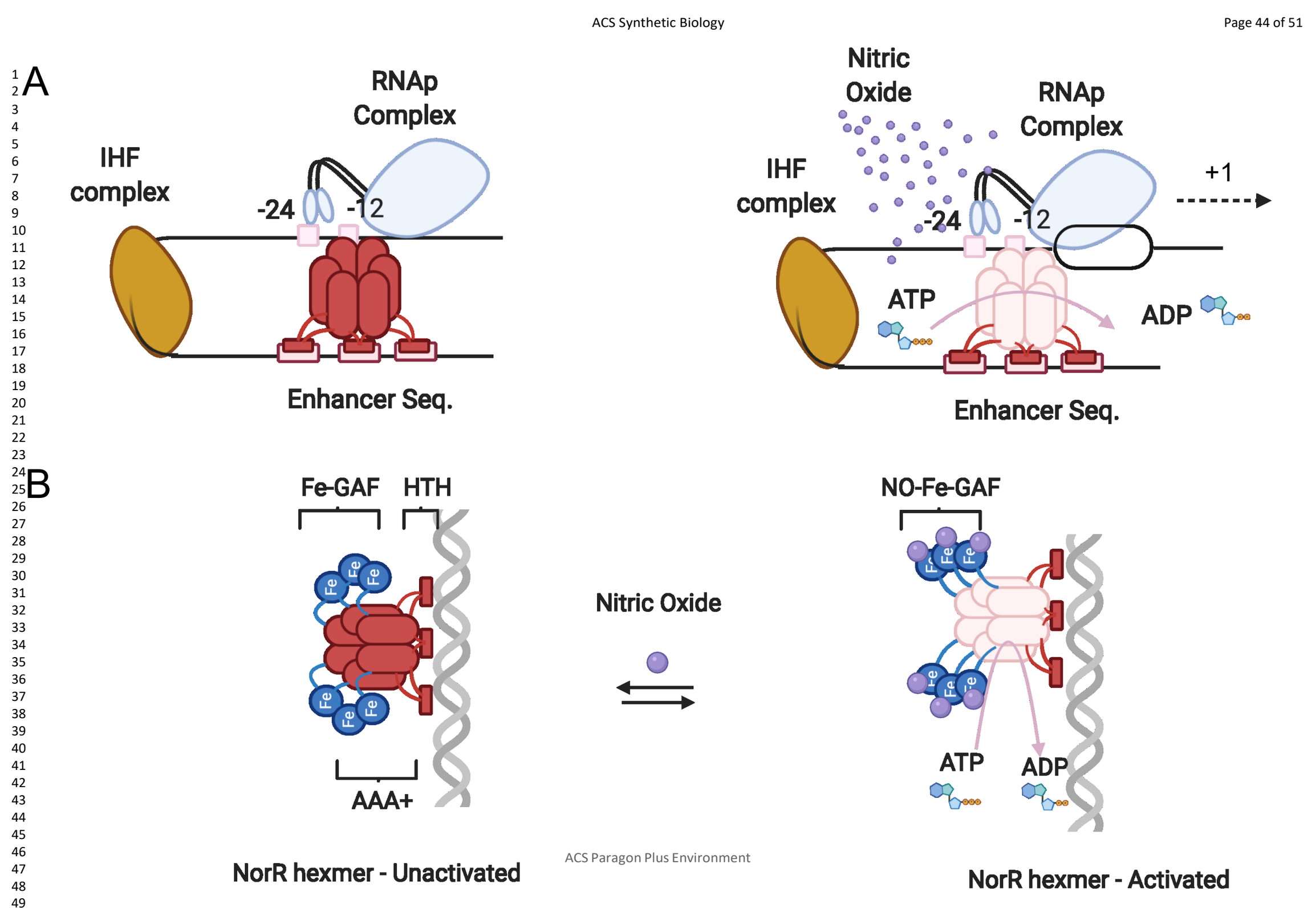
A
RNAp Complex
IHF complex
-24
-12
Enhancer Seq.
Nitric Oxide
RNAp Complex
IHF complex
+1
-24
-12
ATP
ADP
Enhancer Seq.
B
Fe-GAF
HTH
AAA+
NorR hexmer - Unactivated
Nitric Oxide
NO-Fe-GAF
ATP
ADP
NorR hexmer - Activated

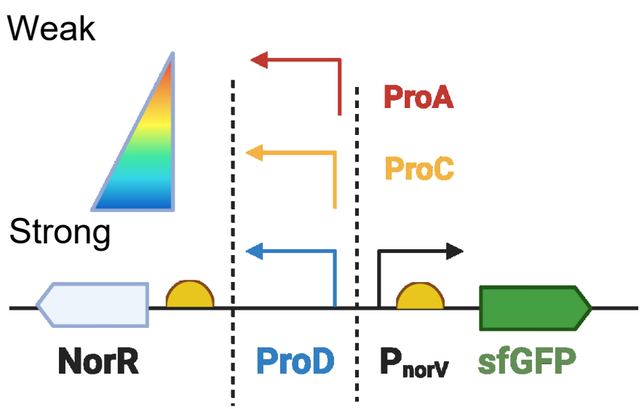
A
Weak
Strong
ProA
ProC
NorR
ProD
P norV
sfGFP
E. coli Nissle 1917

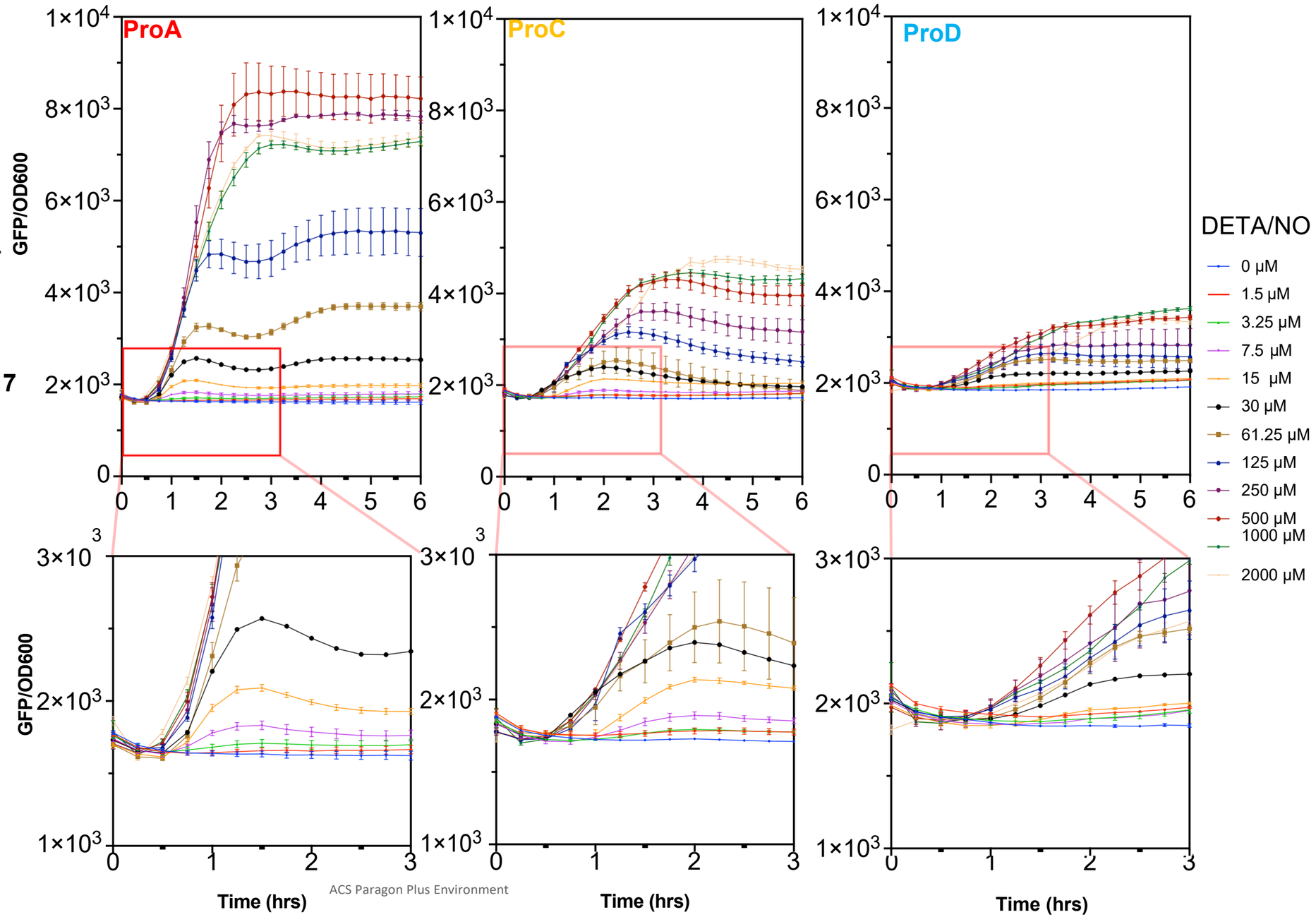
B
ProA
ProC
ProD
GFP/OD600
Time (hrs)
DETA/NO
0 μM
1.5 μM
3.25 μM
7.5 μM
15 μM
30 μM
61.25 μM
125 μM
250 μM
500 μM
1000 μM
2000 μM

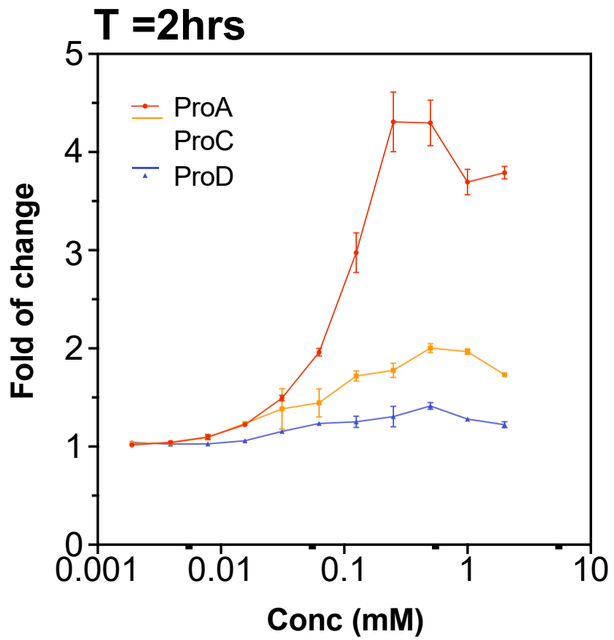
C
T =2hrs
ProA
ProC
ProD
Fold of change
Conc (mM)

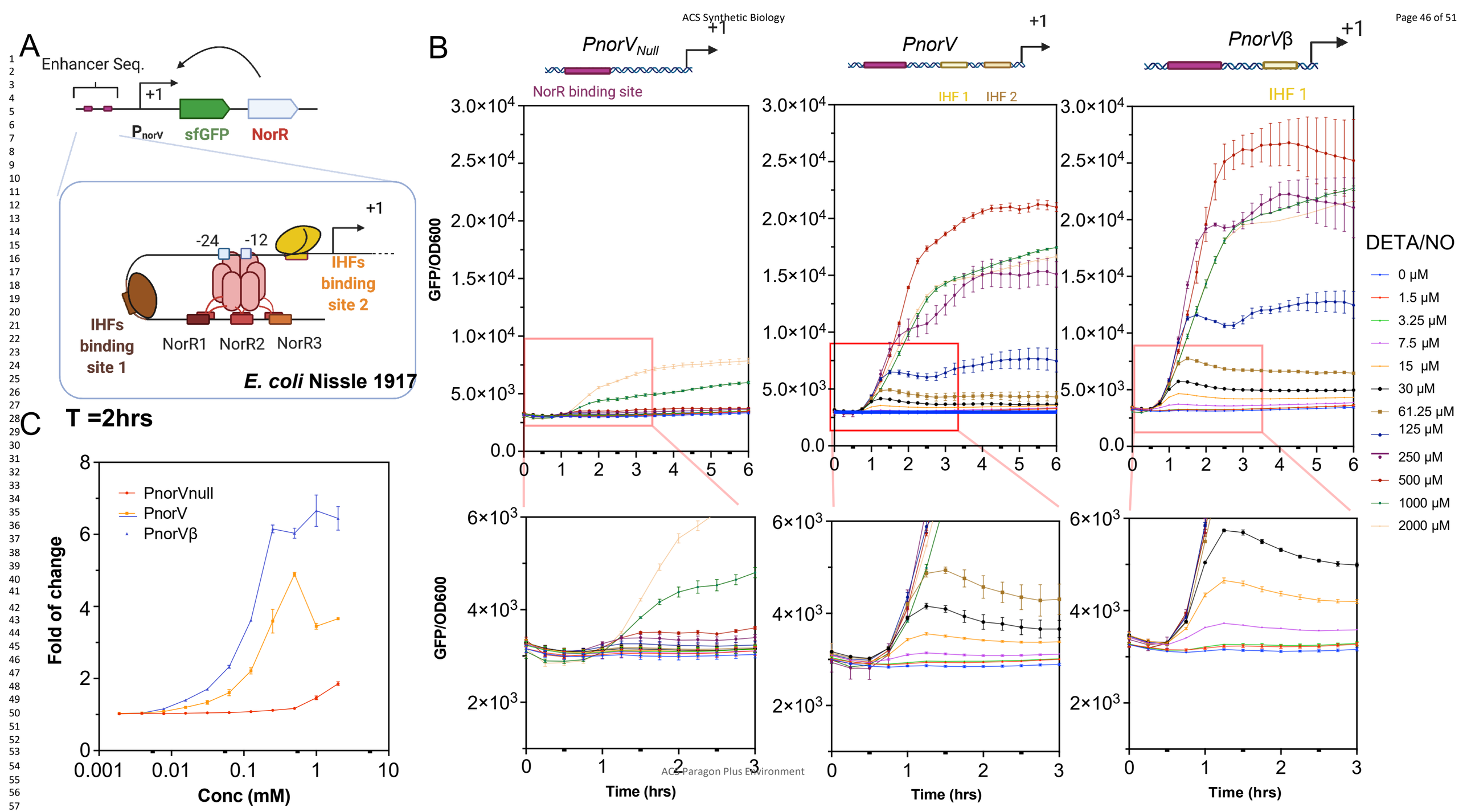
A
Enhancer Seq.
+1
Pnorv
sfGFP
NorR
+1
-24
-12
IHFs binding site 2
IHFs binding site 1
NorR1
NorR2
NorR3
E. coli Nissle 1917
B
PnorV Null
+1
PnorV
+1
PnorVβ
+1
NorR binding site
IHF 1
IHF 2
IHF 1
GFP/OD600
Time (hrs)
DETA/NO
0 μM
1.5 μM
3.25 μM
7.5 μM
15 μM
30 μM
61.25 μM
125 μM
250 μM
500 μM
1000 μM
2000 μM
C
T =2hrs
PnorVnull
PnorV
PnorVβ
Fold of change
Conc (mM)

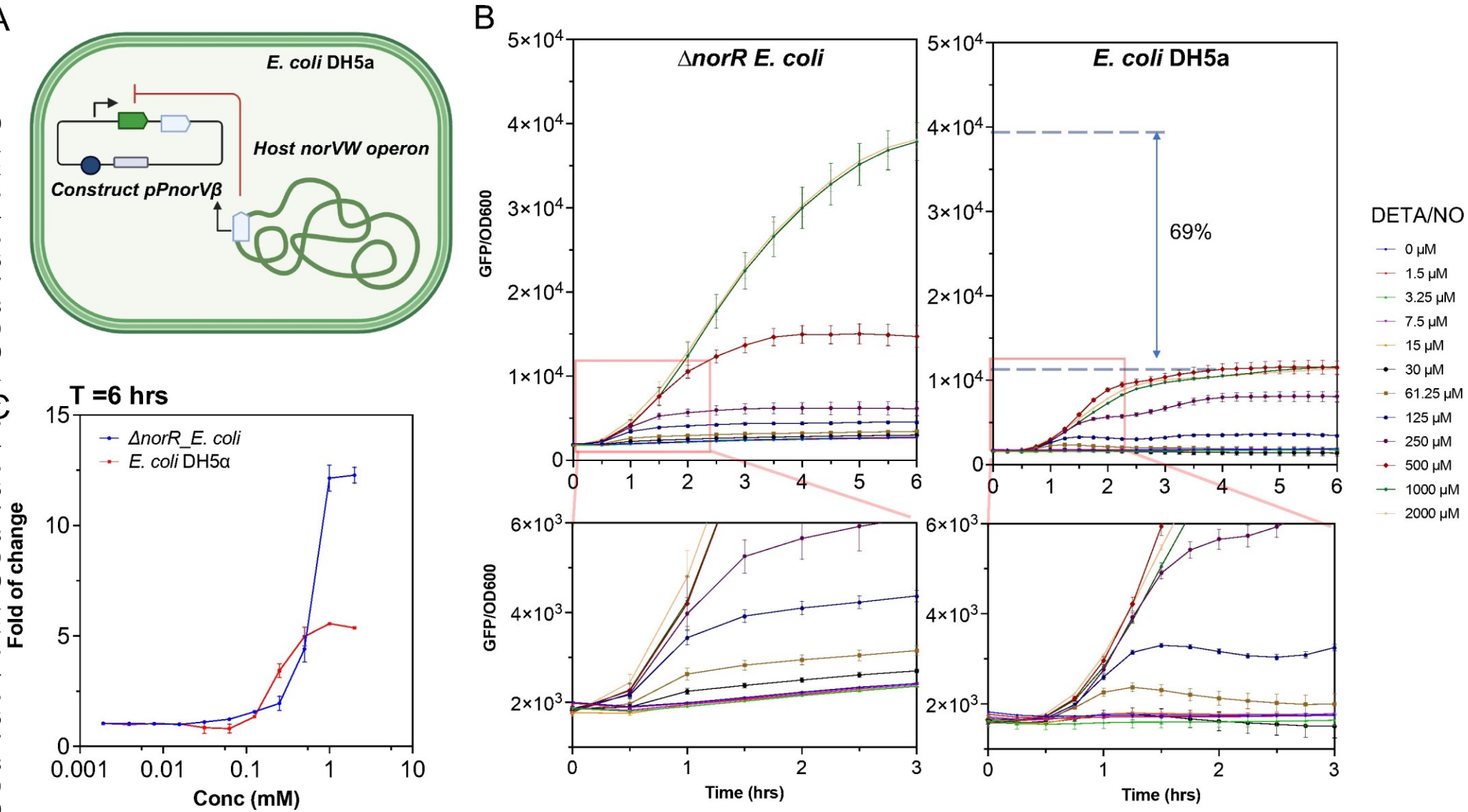
A
E. coli DH5a
Host norVW operon
Construct pPnorVβ
B
ΔnorR E. coli
E. coli DH5a
GFP/OD600
Time (hrs)
69%
DETA/NO
0 μM
1.5 μM
3.25 μM
7.5 μM
15 μM
30 μM
61.25 μM
125 μM
250 μM
500 μM
1000 μM
2000 μM
C
T =6 hrs
ΔnorR_E. coli
E. coli DH5α
Fold of change
Conc (mM)

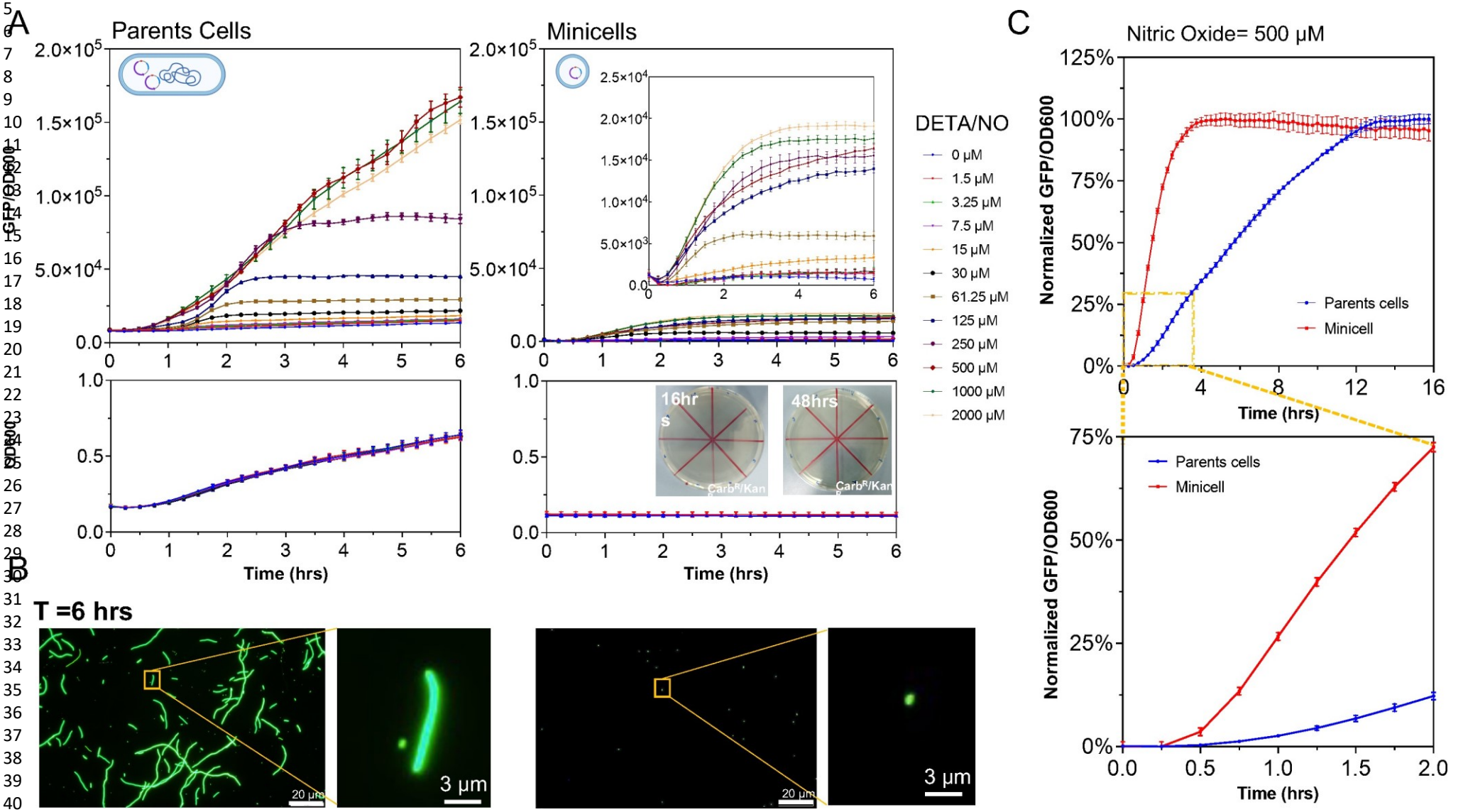
A
Parents Cells
Minicells
GFP/OD600
OD600
Time (hrs)
DETA/NO
0 µM
1.5 µM
3.25 µM
7.5 µM
15 µM
30 µM
61.25 µM
125 µM
250 µM
500 µM
1000 µM
2000 µM
16hrs
48hrs
B
T =6 hrs
20 µm
3 µm
C
Nitric Oxide= 500 µM
Normalized GFP/OD600
Parents cells
Minicell
Time (hrs)

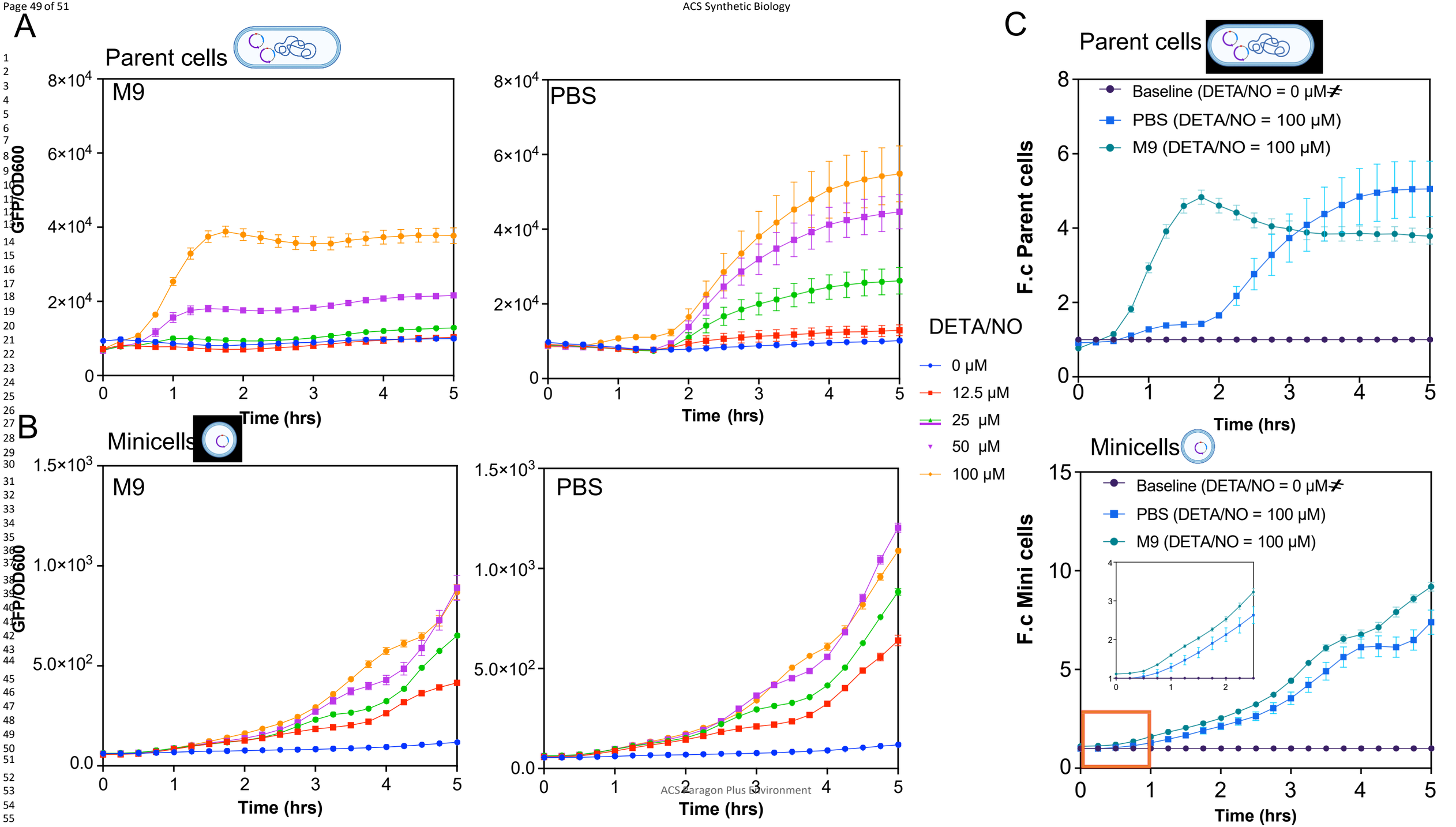

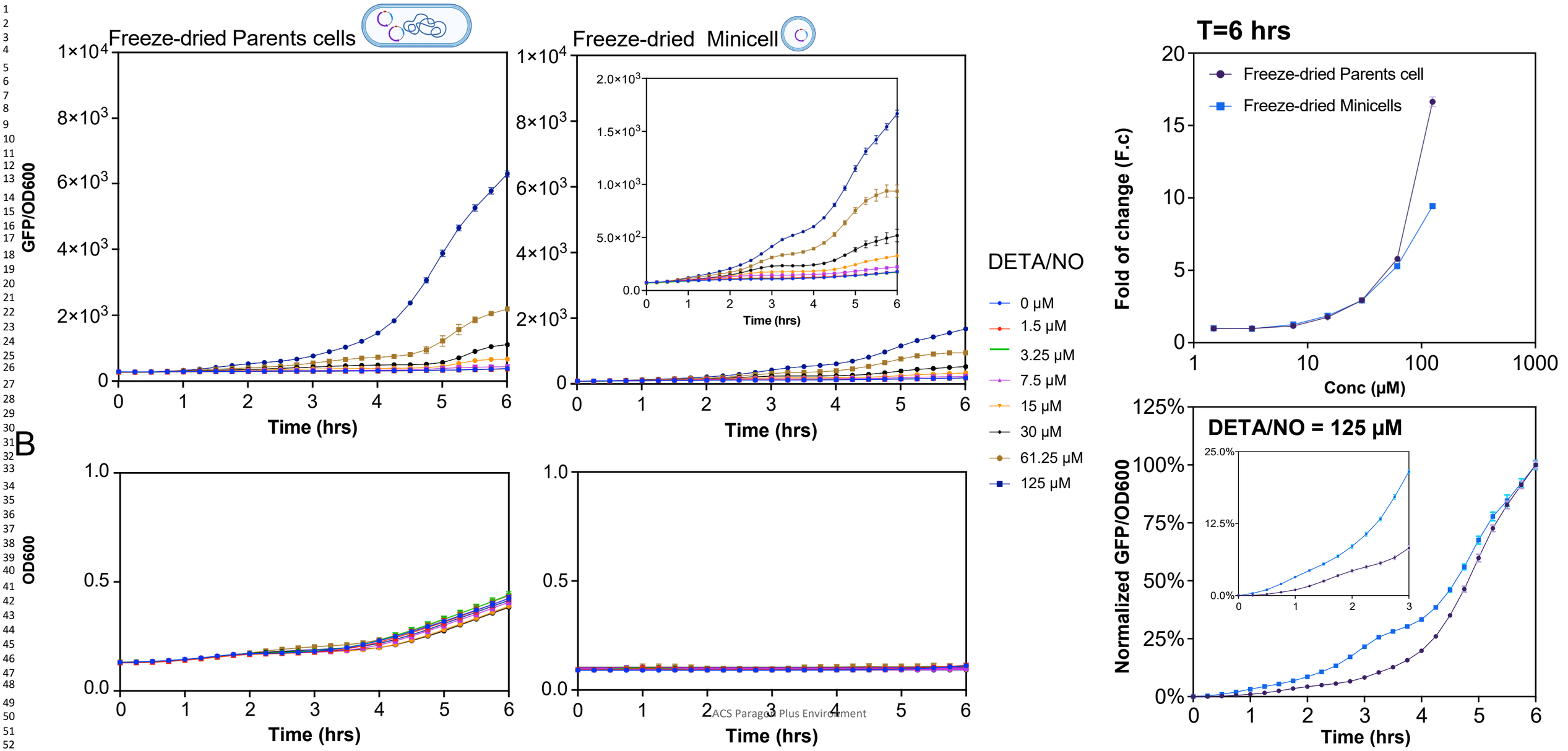

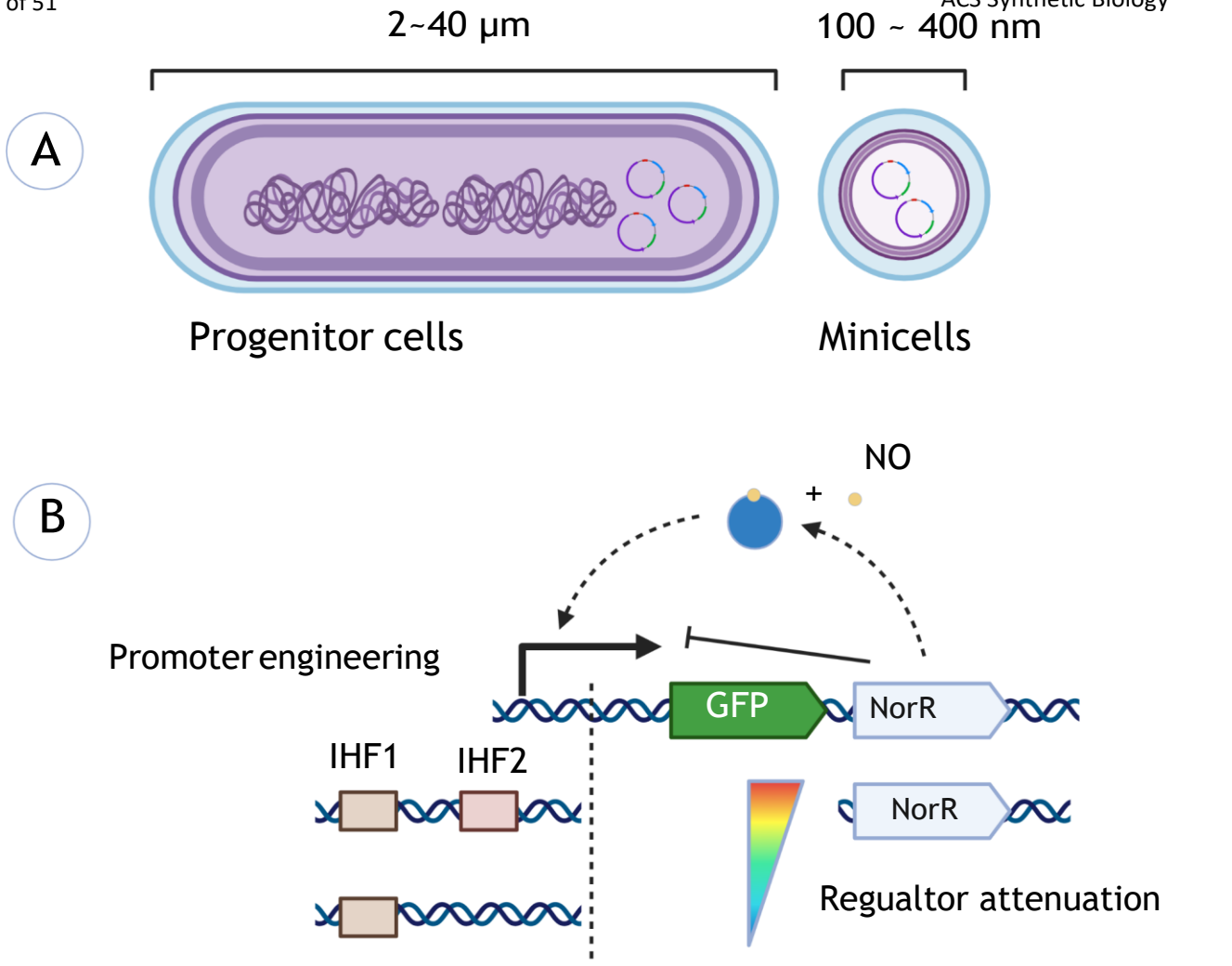
2~40 μm
100 ~ 400 nm
A
Progenitor cells
Minicells
B
NO
+
Promoter engineering
GFP
NorR
IHF1
IHF2
NorR
Regualtor attenuation

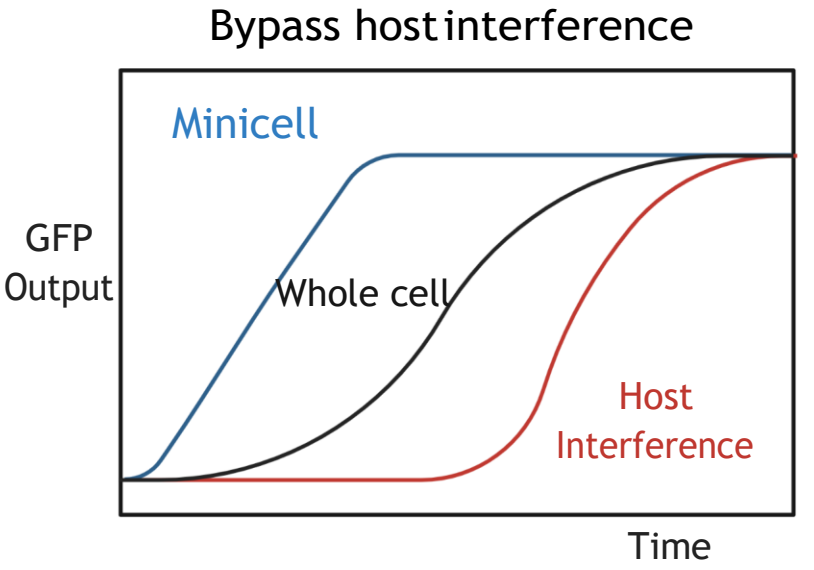
Bypass host interference
Minicell
GFP
Output
Whole cell
Host
Interference
Time

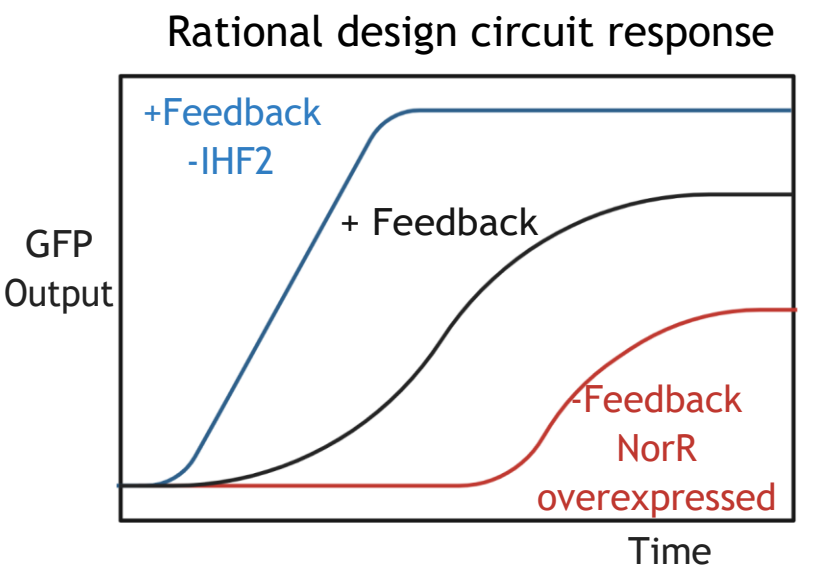
Rational design circuit response
+Feedback
-IHF2
+ Feedback
GFP
Output
-Feedback
NorR
overexpressed
Time